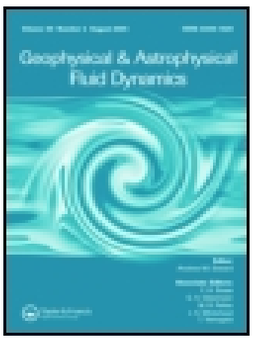

Geophysical & Astrophysical Fluid Dynamics

ISSN: 0016-7991 (Print) (Online) Journal homepage: https://www.tandfonline.com/loi/ggaf19

Space-Time scales of internal waves

Christopher Garrett & Walter Munk

To cite this article: Christopher Garrett & Walter Munk (1972) Space-Time scales of internal waves, Geophysical & Astrophysical Fluid Dynamics, 3:1, 225-264, DOI: 10.1080/03091927208236082

To link to this article: https://doi.org/10.1080/03091927208236082

Published online: 12 Sep 2006.

Geophysical Fluid Dynamics, 1972, Vol. 2, pp. 225–264

Printed in Great Britain

Space-Time Scales of Internal Waves†

CHRISTOPHER GARRETT‡ and WALTER MUNK

Institute of Geophysics and Planetary Physics
Scripps Institution of Oceanography
University of California, La Jolla, California, U.S.A.

(*Received May 19, 1971*).

We have contrived a model $E(\alpha, \omega) \propto \mu^{-1}\omega^{-p+1}(\omega^2-\omega_i^2)^{-\frac{1}{2}}$ for the distribution of internal wave energy in horizontal wavenumber, frequency-space, with wavenumber α extending to some upper limit $\mu(\omega) \propto \omega^{r-1}(\omega^2-\omega_i^2)^{\frac{1}{2}}$, and frequency ω extending from the inertial frequency ω_i to the local Väisälä frequency $n(y)$. The spectrum is portrayed as an equivalent continuum to which the modal structure (if it exists) is not vital. We assume horizontal isotropy, $E(\alpha, \omega) = 2\pi\alpha E(\alpha_1, \alpha_2, \omega)$, with α_1, α_2 designating components of α. Certain moments of $E(\alpha_1, \alpha_2, \omega)$ can be derived from observations. (i) Moored (or freely floating) devices measuring horizontal current $u(t)$, vertical displacement $\zeta(t)$,..., yield the frequency spectra $F_{(u,\zeta,\ldots)}(\omega) = \iint (U^2, Z^2, \ldots)E(\alpha_1, \alpha_2, \omega)\, d\alpha_1\, d\alpha_2$, where $U, Z, \ldots$ are the appropriate wave functions. (ii) Similarly towed measurements give the wavenumber spectrum $F_{(\ldots)}(\alpha_1) = \iint \ldots d\alpha_2\, d\omega$. (iii) Moored measurements horizontally separated by X yield the coherence spectrum $\boldsymbol{R}(X, \omega)$ which is related to the horizontal cosine transform $\iint E(\alpha_1, \alpha_2\ \omega) \cos \alpha_1 X\, d\alpha_1\, d\alpha_2$. (iv) Moored measurements vertically separated by Y yield $\boldsymbol{R}(Y, \omega)$ and (v) towed measurements vertically separated yield $\boldsymbol{R}(Y, \alpha_1)$, and these are related to similar vertical Fourier transforms. Away from inertial frequencies, our model $E(\alpha, \omega) \propto \omega^{-p-r}$ for $\alpha \leqq \mu \propto \omega^r$, yields $F(\omega) \propto \omega^{-p}$, $F(\alpha_1) \propto \alpha_1{}^{-q}$, with $q = (p+r-1)/r$. The observed moored and towed spectra suggest p and q between 5/3 and 2, yielding r between 2/3 and 3/2, inconsistent with a value of $r = 2$ derived from Webster's measurements of moored vertical coherence. We ascribe Webster's result to the oceanic fine-structure. Our choice $(p, q, r) = (2, 2, 1)$ is then not inconsistent with existing evidence. The spectrum is $E(\alpha, \omega) \propto \omega^{-1}(\omega^2-\omega_i^2)^{-1}$, and the α-bandwith $\mu \propto (\omega^2-\omega_i^2)^{\frac{1}{2}}$ is equivalent to about 20 modes. Finally, we consider the frequency-of-encounter spectra $F(\sigma)$ at any towing speed S, approaching $F(\omega)$ as $S \ll S_0$, and $F(\alpha_1)$ for $\alpha_1 = \sigma/S$ as $S \gg S_0$, where $S_0 = 0$(1 km/h) is the relevant Doppler velocity scale.

Introduction

Fluctuations in the vertical structure of temperature and salinity were discovered by Helland-Hansen and Nansen soon after the turn of the century. Subsequently, they were observed on many of the major expeditions (*Michael Sars* in 1910; *Meteor* in 1927 and 1938; *Snellius* in 1929-30); in fact, whenever

† This work has been supported by the National Science Foundation and the Office of Naval Research.

‡ Present address: Department of Oceanography, Dalhousie University, Halifax, Nova Scotia.

a station was repeatedly occupied. A comprehensive account has been given by Defant (1961, Chapter 16).

The early observations consisted of repeated lowerings of Nansen bottles and current meters, and were thus incapable of resolving anything but the very low frequencies. Accordingly, most of the discussion dealt with tidal components. Two principal conclusions emerged:

(i) Observed oscillations of velocity could be reconciled with those of density under the supposition that both were due to internal waves (the prerequisite theory goes back to Stokes in 1847 and Greenhill in 1887); and

(ii) the observed structure is too complex to be interpreted in terms of the fundamental mode only, or even the first two or three modes.

The historical emphasis on mode number rather than horizontal wavenumber is a consequence of the comparative ease of installing vertical arrays. But in any event, the extensive discussions as to whether the first five or seven modes are excited seem beside the point: observations at j depths, each giving the amplitude and phase of some discrete frequency component, can be perfectly fitted by superposition of any j modes.

The development of the bathythermograph in 1940 made it possible to repeat soundings at intervals of minutes rather than hours. It was discovered that high-frequency internal oscillations were also present, all the way to an upper limit determined by the local buoyancy of the water column. At about the same time the concepts of stationary time series were being successfully applied to ocean surface waves, and it became clear that internal waves, too, occupy a frequency continuum (over some six octaves extending from inertial to buoyant frequencies). This point of view was pioneered by Cox (1962, 1967), but there was little progress in sorting out the modal (or wavenumber) structure over this enormously extended frequency domain. Yet there is hardly a problem involving internal waves for which some understanding of the space as well as time scales is not prerequisite.

1. Dispersion

Governing Equations

The linearized equations of motion [with y downwards] are†

$$\frac{\partial \hat{u}_1}{\partial \hat{t}} + \hat{\omega}_i \hat{u}_2 + \frac{1}{\hat{\rho}_0}\frac{\partial \hat{p}}{\partial \hat{x}_1} = 0, \qquad \frac{\partial \hat{u}_2}{\partial \hat{t}} - \hat{\omega}_i \hat{u}_1 + \frac{1}{\hat{\rho}_0}\frac{\partial \hat{p}}{\partial \hat{x}_2} = 0$$

$$\frac{\partial \hat{v}}{\partial \hat{t}} + \frac{1}{\hat{\rho}_0}\frac{\partial \hat{p}}{\partial \hat{y}} + 4\pi^2 \hat{n}^2(y)\,\hat{\zeta} = 0, \qquad \hat{n} = \frac{1}{2\pi}\sqrt{\left(\frac{\hat{g}}{\hat{\rho}_0}\frac{d\hat{\rho}}{d\hat{y}}\right)} \tag{1.1}$$

$$\frac{\partial \hat{u}_1}{\partial \hat{x}_1} + \frac{\partial \hat{u}_2}{\partial \hat{x}_2} + \frac{\partial \hat{v}}{\partial \hat{y}} = 0$$

† Our notation is listed at the end of the paper.

where $\hat{n}(y)$ is the local Väisälä (or buoyancy) frequency in *cycles* per unit time, with $d\hat{\rho}/d\hat{y}$ designating the undisturbed "potential" density gradient ($d\hat{\rho}/d\hat{y} = 0$ for adiabatic compression). We have neglected the horizontal component of rotation and made the Boussinesq approximation (Phillips 1966, §5.7).

We adopt the following scaling:

$$x = 2\pi\hat{M}\hat{x}, \qquad t = 2\pi\hat{N}\hat{t},$$

$$\alpha = \hat{\alpha}/\hat{M} \qquad \omega = \hat{\omega}/\hat{N}, \qquad n = \hat{n}/\hat{N}, \qquad \text{etc.}$$

with $\hat{M}, \hat{N}$ designating as yet unspecified spatial and temporal frequency scales.

Modes propagating horizontally in the direction ϕ have dependent variables

$$\begin{bmatrix} \hat{u}_1 \\ \hat{u}_2 \\ \hat{v} \\ \hat{\zeta} \end{bmatrix} = \mathrm{Re} \begin{bmatrix} iU_L(y)\cos\phi - U_T(y)\sin\phi \\ iU_L(y)\sin\phi + U_T(y)\cos\phi \\ V(y) \\ \dfrac{i}{2\pi\hat{N}} Z(y) \end{bmatrix} \hat{q} \exp\left[i(\alpha_1 x_1 + \alpha_2 x_2 - \omega t)\right] \tag{1.2}$$

U_L, U_T, V, Z are real (dimensionless) functions of y. Hence (Eckart 1960, §51; Phillips 1966, Eq. 5.7.3)

$$\frac{d^2V}{dy^2} + \beta^2 V = 0, \qquad \beta^2(y) = \alpha^2 \frac{n^2(y) - \omega^2}{\omega^2 - \omega_i^2} \tag{1.3}$$

with the usual boundary conditions

$$V = 0 \qquad \text{at} \qquad y = -d \text{ (surface)}, \qquad y = h \text{ (bottom)}. \tag{1.4}$$

The equations of motion require continuity of V and dV/dy at discontinuities of $n^2(y)$.† Set $\alpha = \kappa\cos\theta$, $\beta = \kappa\sin\theta$. Then (Eq. 1.3, r.h.s.)

$$\omega^2 = n^2\cos^2\theta + \omega_i^2\sin^2\theta, \tag{1.5}$$

and if θ is real this relates frequency to the inclination of the propagating vector. A convenient notation is

$$a = \alpha(1 - \omega_i^2/\omega^2)^{-\frac{1}{2}}, \qquad k = an/\omega \tag{1.6}$$

† This assumes n^2 to be finite. In the presence of fine-structure (§7) n^2 is quasi-infinite at the "sheets", and dV/dy is quasi-discontinuous.

so that

$$\beta^2 = a^2[n^2(y)-\omega^2]/\omega^2 = k^2-a^2. \tag{1.7}$$

For $\omega_i = 0$, $k(a, \beta)$ is the wavenumber.

MODEL

So far the discussion does not specify the form of $n(y)$. For definiteness, we take a mixed layer above an exponentially stratified ocean:

$$\hat{n} = 0, \; -\hat{d} < \hat{y} < 0; \qquad \hat{n} = \hat{N}\, e^{-\hat{y}/\hat{b}}, \; 0 < \hat{y} < \hat{h} \tag{1.8}$$

(see Figure 2, left). This not a bad fit to the stability of the world's oceans below 1 km, as compiled by Reid and Lynn (see Figure 1). Just beneath the thermocline our model underestimates $n(y)$. Cox and Sandstrom (1962) fit

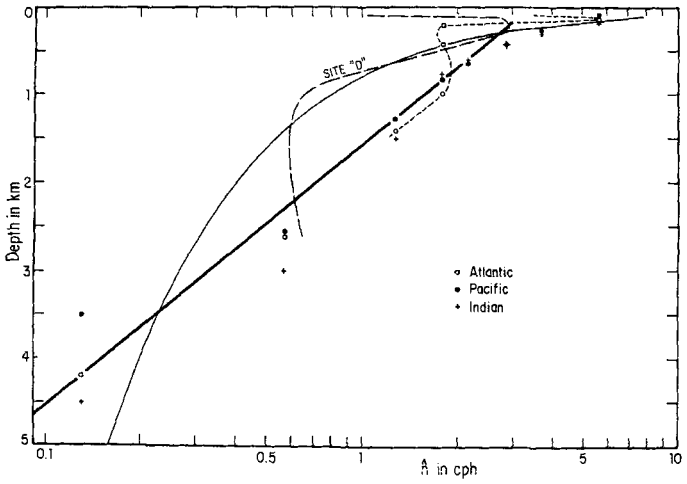

FIGURE 1 Points show typical stratification beneath the thermocline at mid-northern latitudes in the Atlantic, Pacific and Indian oceans (adapted from Reid and Lynn, 1971). The heavy dashed curve shows the somewhat anomalous situation at Atlantic site "D" (Fofonoff, 1969a). Our exponential model $\hat{n} = \hat{N}\, e^{-\hat{y}/\hat{b}}$ (heavy straight line) is drawn for $\hat{N} = 3$ cph, $\hat{b} = 1.3$ km, with $\hat{y}$ designating depth beneath a 200 m. mixed layer. The *local* maximum in $\hat{n}(y)$ varies with time and position but is typically twice the *extrapolated* maximum $\hat{N} = \hat{n}(0)$. In the Pacific and Indian oceans the "super-exponential" rise takes place rather monotonically in the upper few hundred meters; in the North Atlantic (short dashes) a 300 m. minimum is the result of communication with the Polar Sea. A reciprocal relation $\hat{n} = \hat{N}(1+\hat{y}/d)^{-1}$ (solid curve) derived by Monin (1969) and Long (1970) is drawn for $\hat{N} = 8$ cph, and a mixed layer $\hat{d} = 100$ m.

the upper oceans to $\hat{n} = \hat{N}(1+\hat{y}/\hat{d})^{-\frac{1}{2}}$; Monin (1969) and Long (1970) have proposed $\hat{n} = \hat{N}(1+\hat{y}/\hat{d})^{-1}$ from dimensional considerations. As far as this paper is concerned, most of the results can be expressed in terms of the *local* $n(y)$ and it does not much matter which model we take. Equation (1.8) is satisfactory for the bulk of the oceans, and turns out to be analytically convenient.

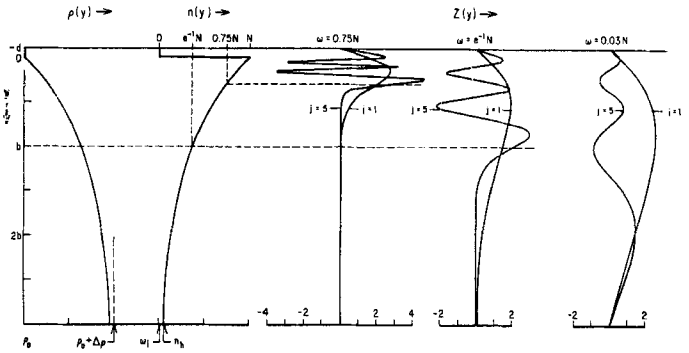

FIGURE 2 The model consists of a mixed layer, $\hat{\rho} = \hat{\rho}_0$, $n = 0$, of thickness $\hat{d}$, above an exponentially stratified ocean $\hat{n} = \hat{N}\, e^{-\hat{y}/\hat{b}}$, where $\hat{n}$ is the Väisälä frequency. The associated distribution of "potential density" is $\hat{\rho} = \hat{\rho}_0 + \Delta\hat{\rho}(1-e^{-2\hat{y}/\hat{b}})$ with $\Delta\hat{\rho} = \frac{1}{2}\hat{\rho}_0\hat{N}^2\hat{b}/\hat{g}$. For the case shown, the thickness, $\hat{d}$, of the mixed layer is 0.1 $\hat{b}$ and the depth beneath the mixed layer is 3 $\hat{b}$. The normalized wave function $Z(y)$ for modes $j = 1$ and 5 at frequencies $\hat{\omega} = \frac{3}{4}\hat{N}$, $e^{-1}\hat{N}$ and $0.03\,\hat{N}$ are shown to the right. For the first two cases the "turning depth" (horizontal dashed lines) are $\hat{b}\ln\frac{4}{3}$ and $\hat{b}$, respectively, well above sea bottom, so that the ocean is essentially of infinite depth; for the third case $\hat{\omega}$ is less than $\hat{n}_h$ (but still above $\hat{\omega}_1$), there is no turning point within the water column, and the effect of finite depth is important.

The stratification depth $\hat{b}$ [1.3 km] and *extrapolated* Väisälä frequency $\hat{N}$ [3 cycles per hour] provide the natural scaling frequencies†:

$$\hat{M} = \hat{b}^{-1}/2\pi = 0.122 \text{ cpkm}, \qquad \hat{N} = \hat{n}(0) = 3 \text{ cph}.$$

Dispersion Relation

The foregoing formulation postulates a simplified density model, a smooth, horizontal, and perfectly reflecting sea floor, neglects nonlinear effects, current shear, etc. Thus the precise features of the normal modes are not applicable, but it is helpful to understand the solution in some detail before retaining such

† Cyclical (rather than circular) frequencies are convenient for subsequent comparison with observations.

gross features as we do believe to be relevant.† (1.3) has solutions

$$V(y) = \sinh a(y+d) \quad \text{for} \quad -d < y < 0, \quad \text{where} \quad n(y) = 0 \tag{1.9}$$

$$V(y) = BJ_a(k) \quad \text{for} \quad 0 < y < h, \quad \text{where} \quad n(y) = e^{-y},$$

defining

$$J_a(k) = J_a(k) - [J_a(k_h)/Y_a(k_h)]\, Y_a(k), \quad k_h = ae^{-h}/\omega, \tag{1.10}$$

in terms of the Bessel functions of the first and second kind of order a. $V(y)$ satisfies the boundary conditions at $y = -d, h$. Continuity of $V, dV/dy$ at $y = 0$ gives the value of B and requires that

$$\tanh ad = -\omega J_a(a/\omega)/J_a'(a/\omega). \tag{1.11}$$

This, together with $a = \alpha(1-\omega_i^2/\omega^2)^{-\frac{1}{2}}$, from (1.6), yields the dispersion relations $\alpha = \alpha^{(j)}(\omega)$.

Effect of rotation Rotation enters the dispersion relation only through the dependence of a on ω_i in (1.6) and leads to an expansion of the horizontal wave length which is appreciable only near inertial frequencies and brings α to zero at $\omega = \omega_i$ for all modes.

Effect of the mixed layer For small d the solutions to (1.11) are

$$a/\omega = z^{(j)}(1-d+0(d^2)) \tag{1.12}$$

if $ad \ll 1$, where $z^{(j)}$ is the jth zero of $J_a(a/\omega)$. If ad is not small, the correction to $z^{(j)}$ is even less. In all further work we take $d = 0$. The dispersion relation is then

$$J_a(k_0)\, Y_a(k_h) - Y_a(k_0) J_a(k_h) = 0, \quad k_0 = a/\omega, \quad k_h = a\, e^{-h}/\omega. \tag{1.13}$$

Effect of finite depth If $\omega \gg n_h = e^{-h}$, then $|Y_a(k_h)| \gg 1$ and (1.13) reduces to

$$J_a(k_0) = 0. \tag{1.14}$$

If in addition $\omega \ll 1$,

$$a/\omega \sim (j-\tfrac{1}{4}+\tfrac{1}{2}a)\pi \tag{1.15}$$

For ω close to ω_i we cannot neglect the effect of finite depth, but let us suppose (and check later) that $k_h \gg 1$ so that we may use the asymptotic forms

† The essential relations can be derived more directly by a WKBJ approximation, as has been emphasized by a referee (K.H.).

for large arguments of the Bessel functions throughout in (1.13). This yields

$$a/\omega = j\pi/(1-e^{-h}),\dagger \tag{1.16}$$

and $k_h = e^{-h}a/\omega$ is large only if $j\pi$ exceeds e^h. For our model $e^h = 30$ so that (1.16) is valid only for high modes; for *low* modes a/ω will have values between those appropriate to infinite depth (1.15) and to small depth (1.16). Numerical solution of (1.13) for our model actually gives

$$a/\omega = k_i, \qquad k_i = 2.96 \tag{1.17}$$

for the gravest mode near $\omega = \omega_i$, as compared to the bounds 2.36 and 3.25 of (1.15) and (1.16). Equation (1.17) is accurate to within 20% up to $\omega = 0.22$. Accordingly, the dimensional phase speed‡ of the gravest mode away from ω_i is $\hat{\omega}/\hat{\alpha} = (2\sqrt{2}/k_i)\sqrt{(\hat{g}'\hat{b})}$, where $\hat{g}' = \hat{g}\cdot\Delta\hat{\rho}/\hat{\rho} = \frac{1}{2}\hat{b}\hat{N}^2$, is "reduced gravity".

Solution for large wavenumbers For $\omega = 1-\varepsilon$, the dispersion relation may be taken as $J_a(k_0) = 0$ and we may replace a by α. Then $\alpha/\omega = \alpha+\alpha\varepsilon$ and we use the Airy approximation for Bessel functions whose order and argument are nearly the same. For large α

$$J_\alpha(\alpha+z\alpha^{\frac{1}{3}}) = 2^{\frac{1}{3}}\alpha^{-\frac{1}{3}}\,\mathrm{Ai}(-2^{\frac{1}{3}}z)+0(\alpha^{-1}) \tag{1.18}$$

where $z = \varepsilon\alpha^{\frac{2}{3}}$, and so $-2^{\frac{1}{3}}z$ must be a zero of the Airy function.

Thus

$$-2^{\frac{1}{3}}(1-\omega)\alpha^{\frac{2}{3}} = -2.34,\ -4.09,\ldots,\ -\left[\frac{3\pi(4j-1)}{8}\right]^{\frac{2}{3}},\ldots \tag{1.19}$$

hence

$$\alpha^{(j)}(\omega) = c^{(j)}(1-\omega)^{-\frac{2}{3}},\ c^{(j)} = 2.53,\ 5.85,\ldots,\ \frac{3\pi(4j-1)}{8\sqrt{2}}. \tag{1.20}$$

Figure 2 illustrates the wave function $Z(y)$ for various modes and frequencies. The full dispersion relation (1.13) is shown in Figure 3. The essential features in these illustrations are not sensitive to the precise form chosen for $n(y)$: an *inertial* range ($\omega_i \leqq \omega < 2\omega_i$), $\alpha^{(1)} = k_i(\omega^2-\omega_i^2)^{\frac{1}{2}}$, for

† This solution is exact for $a = \frac{1}{2}$.

‡ With a mixed layer the phase speed of the gravest mode is still $0(\sqrt{[\hat{g}'\hat{b}]})$ provided that $\hat{d} \ll \hat{b}$. In the other extreme, namely $\hat{d} \gg \hat{b}$ (i.e. $d \gg 1$), it is $0(\sqrt{[\hat{g}'\hat{d}]})$ for $h \to \infty$. In that case $J_a(k) = J_a(k)$, and (1.11) yields $1/d = -[(a/\omega)J_a'(a/\omega)]/J_a(a/\omega) = -a+\frac{1}{2}(a/\omega)^2+\ldots$ for the gravest mode. Thus, if $ad \ll 1$, $a/\omega = \sqrt{(2/d)}$, or dimensionally, away from ω_i, the phase speed is $\hat{\omega}/\hat{\alpha} = 2\pi\sqrt{(\hat{g}'\hat{d})}$.

which rotational effects are important; a *linear* range ($2\omega_i < \omega < 0.2$), $\alpha^{(1)} \approx k_i\omega$; and a *buoyant* range ($0.7 < \omega \leqq 1$), $\alpha^{(1)} = 2.53\ (1-\omega)^{-\frac{1}{2}}$. The *intermediate* range ($0.2 < \omega < 0.7$) has no single approximation.

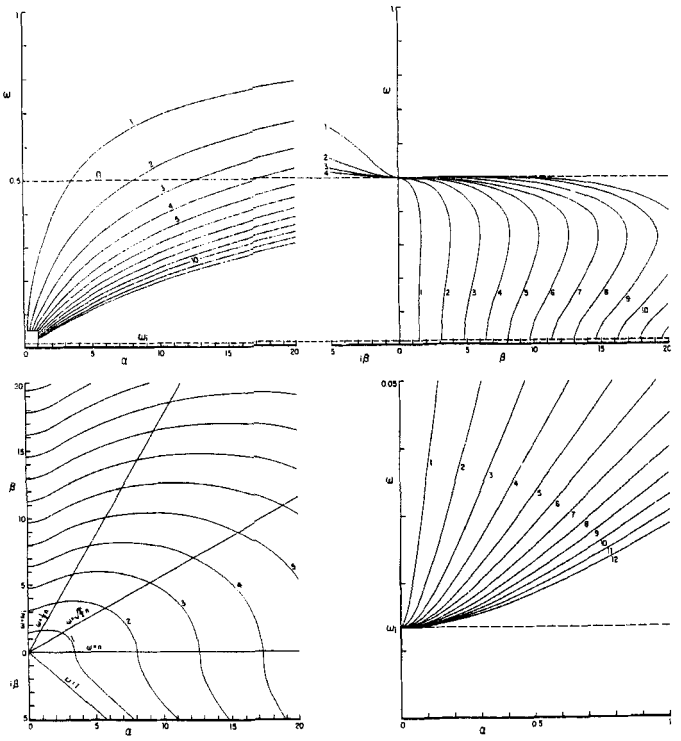

FIGURE 3 Left Top: the dispersion relation $\alpha^{(j)}(\omega)$, $j = 1, 2, \ldots$, (Eq. 1.13) for the case $d = 0$, $h = 4.5$ km/1.3 km $= 3.45$, $n_h = 0.095$ cph/3 cph $= 0.032$, $\omega_l = 0.04$ cph/3 cph $= 0.0133$. The situation near the origin (white box) is drawn on a magnified scale on the right bottom. The left bottom and right top panels give the mode distribution at a depth $y = 0.69$ (for which $n = e^{-y} = 0.5$) in α,β- and ω,β-space, respectively. For $\omega < n(y)$, β (as defined in 1.3) represents the local vertical wavenumber; for $\omega > n(y)$, β is imaginary and $(i\beta)^{-1}$ is the local e-folding scale.

2. Normalization

The wave functions satisfying (1.1) are

$$\begin{bmatrix} U_L(y) \\ \overline{U_T(y)} \\ V(y) \\ Z(y) \end{bmatrix} = \begin{bmatrix} -nJ_a'(k) \\ (\omega_i/\omega)nJ_a'(k) \\ \omega(\alpha/a)J_a(k) \\ (\alpha/a)J_a(k) \end{bmatrix} N(\omega, \alpha) \tag{2.1}$$

where $N(\omega, \alpha)$ is a normalization function derived from the condition

$$\int_0^h [\tfrac{1}{2}(U_L^2+U_T^2+V^2)+\tfrac{1}{2}n^2Z^2]\,dy = 1 \tag{2.2}$$

Now

$$\int_0^h \tfrac{1}{2}(U_L^2+U_T^2+V^2)dy = \tfrac{1}{2}N^2k_0^{-2}\int_{k_h}^{k_0}[(1+\omega_i^2/\omega^2)k^2J_a'^2(k)+a^2J_a^2(k)]k^{-1}\,dk \tag{2.3}$$

$$= \tfrac{1}{2}N^2k_o^{-2}\int_{k_h}^{k_0}[(1+\omega_i^2/\omega^2)k^2-2\omega_i^2k_0^2]J_a^2(k)k^{-1}\,dk \tag{2.4}$$

where we have used $\int kJ_a'^2\,dk = kJ_a'J_a+\int(k^2-a^2)k^{-1}J_a^2\,dk$ from Bessel's equation. The ratio of the two contributions to the integral is

$$\frac{2\omega_i^2k_0^2}{(1+\omega_i^2/\omega^2)k^2} = 2\frac{\omega_i^2}{n^2}\frac{\omega^2}{(\omega^2+\omega_i^2)} \tag{2.5}$$

which equals $(\omega_i/n_h)^2 = \boldsymbol{0}(10^{-1})$ near the bottom, and is even smaller elsewhere, so that the second contribution to the integrand can be neglected.

Also

$$\int_0^h \tfrac{1}{2}n^2Z^2\,dy = \tfrac{1}{2}N^2k_0^{-2}\int_{k_h}^{k_0}(1-\omega_i^2/\omega^2)J_a^2(k)\,kdk, \tag{2.6}$$

hence the ratio of the vertically integrated potential to kinetic energy is $(\omega^2-\omega_i^2)/(\omega^2+\omega_i^2)$. The normalization condition becomes

$$N^2k_0^{-2}\int_{k_h}^{k_0}kJ_a^2(k)\,dk = 1. \tag{2.7}$$

We now use the identity (Luke 11.2(4)) $\int_0^{x_0} xC_a^2(x)\,dx = \tfrac{1}{2}x_0^2C_a'^2(x_0)$ where $C_a(x)$ is any solution of Bessel's equation and $C_a(x_0) = 0$. Hence

$$N = \sqrt{2}[J_a'^2(k_0)-n_h^2J_a'^2(k_h)]^{-\frac{1}{2}} = \tfrac{1}{2}\sqrt{2\pi k_0}[Y_a'^2(k_0)-Y_a'^2(k_h)]^{-\frac{1}{2}}, \tag{2.8}$$

the latter form following from the boundary conditions

$$J_a(k) = J_a(k)-[J_a(k_p)/Y_a(k_p)]Y_a(k)$$

for $p = 0$ or h (Eqs. 1.4, 1.10),

and the identity $J'Y-JY' = -2/(\pi k)$.

The wave functions (2.1) with the normalization (2.8) give us the modal solutions. Above the turning depth these solutions are wiggly, particularly for high modes, and if there are many modes (as will be demonstrated) we may replace the solutions by their mean-square values. This enables us to relate spectra of different variables, both to each other and to the total energy, without retaining details of the stratification or mode structure.

For $\omega \gg n_h$ the second term in either formula (2.8) is negligible, $N = \sqrt{2}/J'_a(a/\omega)$, and $J_a(k) = J_a(k)$. Well above the turning depth (where $\omega = n(y)$) we have then

$$J_a(k)N = \pm \sqrt{(2/n)} \cos(k - \tfrac{1}{2}a\pi - \tfrac{1}{4}\pi), \quad \omega \ll n. \tag{2.9}$$

If we average the wave functions over many wiggles above the turning depth, and take them to be zero below,

$$\left.\begin{aligned} &\overline{U_L^2} = n, \quad \overline{U_T^2} = n(\omega_i/\omega)^2, \quad \overline{V^2} = n^{-1}(\omega^2 - \omega_i^2), \\ &\overline{Z^2} = n^{-1}(\omega^2 - \omega_i^2)/\omega^2 \quad \text{for} \quad \omega \leqq n \\ &\overline{U_L^2} = \overline{U_T^2} = \overline{V^2} = \overline{Z^2} = 0 \quad \text{for} \quad \omega > n. \end{aligned}\right\} \tag{2.10}$$

For $\omega \ll n_h$ we use the asymptotic forms of all the Bessel functions throughout, hence $Y_a^{-2}(k_h) = (k_h/k_0)Y_a^{-2}(k_0)$, so that the second term in (2.8) is again negligible. Thus we obtain

$$J_a(k)N = \pm \sqrt{(2/n)} \sin(k_v - k) \tag{2.11}$$

and (2.10) follows as before. We shall take (2.10) to be uniformly valid, though the derivation is inaccurate for low modes (see (1.16) *et seq.*).

We shall be interested not in U_L^2 and U_T^2 separately, but in the total horizontal velocity U^2. For an elementary wave field, $\exp i\gamma$, $\gamma = \alpha_1 x_1 + \alpha_2 x_2 - \omega t$, traveling in a direction ϕ, we have $u_1 = -U_L \cos\phi \sin\gamma - U_T \sin\phi \cos\gamma$, $u_2 = -U_L \sin\phi \sin\gamma + U_T \cos\phi \cos\gamma$, hence

$$u^2 = u_1^2 + u_2^2 = U_L^2 \sin^2\gamma + U_T^2 \cos^2\gamma. \tag{2.12}$$

An average over wave phase γ is $\overline{u^2} = \frac{1}{2}(U_L^2 + U_T^2) = \frac{1}{2}U^2$, and so, as might have been expected,

$$\overline{U^2} = \overline{U_L^2} + \overline{U_T^2} = n(\omega^2 + \omega_i^2)/\omega^2 \quad \text{for} \quad \omega \leqq n; \quad \overline{U^2} = 0 \quad \text{for} \quad \omega > n. \tag{2.13}$$

The derived mean-square quantities are simple, depend only on ω (and not on α), and the stratification model enters only through an explicit dependence on local n. These advantages are achieved at the expense of the normalization condition, for

$$\begin{aligned} \int_0^h [\tfrac{1}{2}(\overline{U^2} + \overline{V^2}) + \tfrac{1}{2}n^2\overline{Z^2}]\, dy &= \int_w^1 [1 + \tfrac{1}{2}n^{-2}(\omega^2 - \omega_i^2)]\, dn \\ &= (1-w)[1 + \tfrac{1}{2}w^{-1}(\omega^2 - \omega_i^2)], \end{aligned} \tag{2.14}$$

instead of 1 (Eq. 2.2), where $w = \max(\omega, n_h)$. There are three contributions to this error:

(i) The asymptotic approximation to $J_a(k)$ for large argument is not valid near the turning point, and becomes increasingly poor as $\omega \to 1$.

(ii) If the turning point is near the surface, i.e., $n(y) \doteqdot 1$, our asymptotic approximation to the normalization constant N is also poor.

(iii) For small ω the neglect of the second contribution to the integrand in (2.4) introduces a small error.

The approximations for $\omega \approx n(y)$ could be improved by using the Airy approximation for $J_a(k)$, and also for N if necessary, but only with substantial loss of simplicity. We shall use the formulae (2.10, 12), bearing in mind that they will not be accurate for $\omega \approx n(y)$, particularly if $n(y) \approx 1$.

The local ratio of potential to horizontal kinetic energy is $\frac{1}{2}n^2\overline{Z^2}/\frac{1}{2}\overline{U^2} = (\omega^2-\omega_i^2)/(\omega^2+\omega_i^2)$. Fofonoff (1969a) obtains $n^2/(n^2-\omega^2)$ times this ratio for plane waves in a region of constant n. But unless n is constant from top to bottom, the infinity in Fofonoff's energy ratio at $\omega = n$ is spurious, as the associated large vertical scale in the wave function near $\omega = n$ must be inappropriate to a *WKBJ* approximation. Our ratio of approximately 1, while inaccurate near the turning point, seems preferable, and is in fact in good agreement with an Airy approximation based on our final model, and with Fofonoff's Figure 1.

3. The observed spectra

Moored Spectra

The most complete observations yet made are the current measurements by Fofonoff and Webster at site "D" in the western North Atlantic (Fofonoff 1966, 1969b; Webster 1968a, b). Spectra $F_u(\omega)$ have a similar ω-dependence at all depths but intensities that increase by about 10 db from the deep (2000 m) to the shallow (50 m) stations. The spectra can be concentrated into a 3 db band by dividing with the local $n(y)$ (Fofonoff, 1969b), consistent with the *WKBJ* result that $u \propto n^{\frac{1}{2}}(y)$ (Eq. 2.13). Vital statistics are given in Table I, and the results are plotted in Figure 4. The site "D" spectra lie between Bay of Biscay (Gould, personal communication) and Mediterranean spectra (Perkins, 1970). The Mediterranean and site "D" spectra are sharply cusped at the local inertial frequency; the Bay of Biscay spectra peak at the M_2 frequency and on the continental slope show subsidiary peaks at $2M_2$, $3M_2$,... The Bermuda spectra (Fofonoff 1966, 1969b, Webster, 1970) are unique with regard to the low ambient noise level, permitting the spectra to be detected to almost 10^3 cph along an extension of the ω^{-2} band shown in the figure.

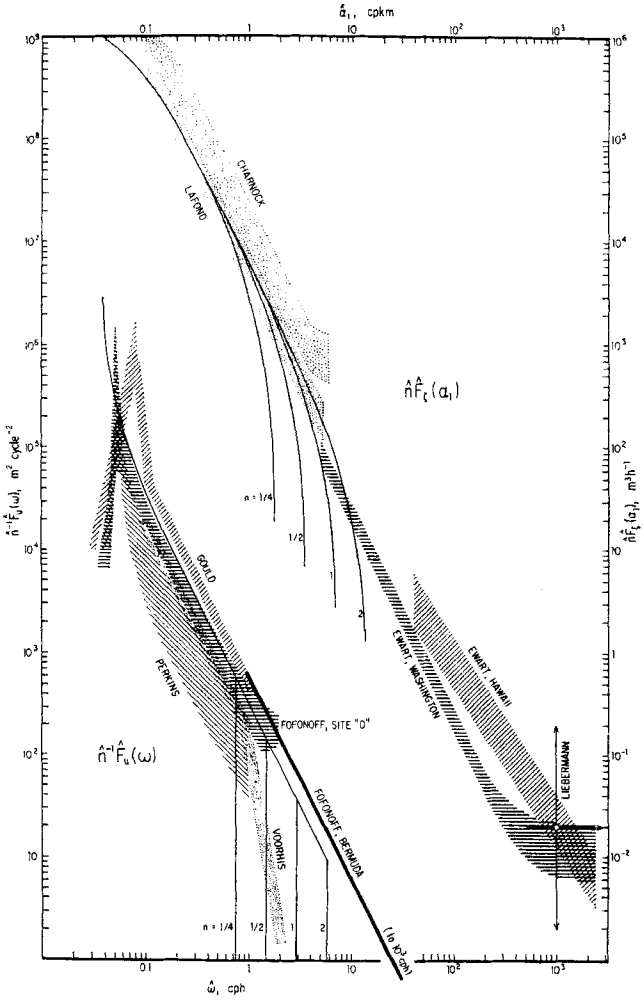

FIGURE 4 Bands represent the observed moored and floating spectra (Left, see Table 1) and towed spectra (Right, see Table 2). Dotted bands are presumably not subject to fine-structure noise. Curves are the derived relations (6.20, 21).

We also show comparable spectra based on measurements of vertical flow† from neutrally buoyant floats (Voorhis, 1968). The "floating spectra" cut off sharply above their respective local Väisälä frequencies.

† Voorhis plots the spectrum of potential energy, $\hat{P}(\omega) = \frac{1}{2}\rho(2\pi\hat{n})^2\hat{F}(\omega)$, in units of ergs cm^{-3}/cph. Thus $\hat{F}_\zeta = 2(2\pi\hat{n})^{-2}\,\hat{P}$ (cm/sec)^2/cph $= 2(2\pi\hat{n})^{-2}\,(36)^2\,P$ (m/h)^2/cph, and $\hat{n}^{-1}\hat{F}_u = 4\pi^2\hat{n}(\omega^2+\omega_i^2)(\omega^2-\omega_i^2)^{-1}\hat{F}_\zeta = 2(36)^2(\omega^2+\omega_i^2)(\omega^2-\omega_i^2)^{-1}\hat{n}^{-1}\hat{P}m^2$, with $\hat{n}$ in cph. This relates the ordinate $\hat{P}$ of Voorhis' Figure 5 with $\hat{n}^{-1}\hat{F}_u$ of Figure. 4.

TABLE I

Parameters for moored and floating spectra. d is thermocline depth, h ocean depth, y instrument depth, $n(y)$ Väisälä frequency, T typical record length.

	Fofonoff–Webster		*Gould*		*Perkins*		*Voorhis*	
	←——————Moored current meters——————→						Neutral float	
	N.W. Atlantic		Bermuda		Bay of Biscay		Mediterranean		Off New England	
	39°N 70°W		32°N 64°W		46°N 8°W		38°N 5°E		39°N 71°W	
d, h	50 m, 2640 m		100 m, 2500 m		50 m, 5000 m		50 m, 2830 m		50 m, 2600 m	
T	months		3 days		2 weeks		2 months		3–5 days	
	y	$n(y)$	y	$n(y)$	y	$n(y)$	y	$n(y)$	y	$n(y)$
	50 m	3.12 cph	494 m	2 cph	350 m	1.1 cph	200 m	2.1 cph	390 m	2.3 cph
	106	3.03			410	1.1	700	1.1	725	1.0
	511	1.48			1400	1.3	1200	1.1	960	0.7
	1013	0.66					1700	1.1		
	1950	0.58					2200	1.1		

Towed Spectra

Charnock (1965) and LaFond and LaFond (1971) have analyzed the vertical displacements of specified isotherms from records of thermistor chains towed behind vessels (Table II, Figure 4). LaFond's chain consists of 34 (!) sensors at 8 m vertical separation. The depth of a particular isotherm is found by interpolation. Ewart (personal communication) has measured temperature at fixed depths up to 2500 m with a sensor mounted on a self-propelled "isobaric" vehicle, and from these he obtains the temperature spectra $F_T(\alpha_1)$. In order to compare these to the displacement spectra of Charnock and LaFond we divide by $(dT/dy)^2$, the squared (potential) temperature gradient at the mean depth of the selected isotherms.† We plot $\hat{n}\hat{F}_\zeta(\alpha_1)$ to allow for varying stability with depth (Eq. 2.10). Finally we refer to Liebermann's (1951) measurements with rapid response thermometers mounted on a submarine moving at 2 to 4 knots in 30 to 60 m depths through continental waters from Southern California to Alaska. The range in wavenumbers is

† Writing $d\rho = a\,dT + b\,dS = (a + b\cdot dS/dT)\,dT$, we have $(dT/dy) = (n^2/g)T^*$, $T^* = (\rho/a + b\cdot dS/dT)$, where $S(T)$ is the local salinity–temperature relation. The temperature spectra at a fixed depth are $F_T = (dT/dy)^2 F_\zeta \propto n^4 F_\zeta \propto n^3$ (Eq. 2.10).

roughly 0.1 to 10 cpm†, and the results (shown by a cross) are not inconsistent with the Ewart measurements. Simultaneous tow (depth 100 m) and drogue (75 m) measurements of temperature northwest of Bermuda by Voorhis and

TABLE II

Parameters for towed spectra. C is velocity of tow, L length of tow, d thermocline depth. For Charnock and LaFond, y is the mean depth of isotherm T; for Ewart, y is depth of vehicle, and dT/dy the local temperature gradient. n is Väisälä frequency at depth y.

	Charnock			*LaFond*			*Ewart*					
	Thermistor chain						Fixed depth vehicle					
	Gibraltar			California			Washington			Hawaii		
	34°N 12°W			34°N 120°W			47°N 131°W			20°N 157°W		
C	12 knots			6 knots			5 knots			5 knots		
L	40 km			72 km			10 km			8–16 km		
d	50 m			60 m			surface			200 m		
	y	n	T	y	n	T	y	n	dT/dy	y	n	dT/dy
	65 m	6 cph	20°	66 m	6 cph[a]	18°	338 m	2.7 cph	7.2°/km	494 m	2.3 cph[b]	6.1°/km
	75	6	18°	91	6[a]	15°				1692	0.9[b]	1.7
										2495	0.49[b]	0.6[b]

[a] Computed from CALCOFI Cruise 6612 at station 34°15′N, 119°59′W, 10 Dec. 1966.
[b] Inferred from typical Pacific conditions.

Perkins (1966) are consistent with α^{-2} and ω^{-2} slopes, respectively, and the intensities yield spectra (not plotted) that appear to be of the same order as those in Figure 4.

Coherence

The observational record, starting in 1931 with the measurements by Ekman and Helland-Hansen, consists mostly of expressions of dismay that there should be so little resemblance between oscillations of such long periods measured at such small spatial separation. After forty years we ought to be able to do better!

† Within this band typical r.m.s. fluctuations are $\delta T = 0.02$°C. Liebermann fitted the temperature auto-correlation by $\exp(-\alpha_0 X_1)$, X_1 being the lag distance, and $\alpha_0^{-1} = 0(1\,\text{m})$ the correlation scale. The resulting spectrum is $F_\zeta(\alpha_1) = (dT/dy)^{-2}(\delta T)^2 2\pi^{-1}\alpha_0(\alpha_0^2+\alpha_1^2)^{-1}$, constant for $\alpha_1 \ll \alpha_0$ and proportional to α_1^{-2} for $\alpha_1 \gg \alpha_0$. The plotted value $\hat{n}\hat{F}_\zeta(\alpha_0) = 2\times 10^{-2} m^3 h^{-1}$ is obtained for $\hat{\alpha}_0 = 1$ cpm, $\hat{n} = 6$ cph, $dT/dy = 0.2$°C/m.

To introduce a quantitative measure of resemblance, let $f_m(t)$ be a stationary time series at a point $\boldsymbol{r}_m(x_1, x_2, y)$ for any component of velocity, displacement, etc. Similarly $f_n(t)$ is the time series at $\boldsymbol{r}_n$, not necessarily for the same variable. The time average

$$\rho_{mn}(\tau) = \langle f_m(t) f_n(t+\tau) \rangle \tag{3.1}$$

is called the covariance of the two series. The co-spectrum $C_{mn}(\omega)$ and the quadrature spectrum $Q_{mn}(\omega)$ are defined by

$$C_{mn}(\omega) + iQ_{mn}(\omega) = \frac{2}{\pi} \int_0^\infty \rho_{mn}(\tau)\, e^{-i\omega\tau}\, d\tau. \tag{3.2}$$

ω is restricted to be non-negative. For the special case $m = n$ we have $Q_{mn} = 0$, and $C_{mn} = F_n(\omega)$ is then known as the power spectrum of $f_n(t)$. The coherence, $\boldsymbol{R}_{mn}(\omega)$, and phase lag γ_{mn} of f_n relative to f_m at frequency ω are defined by

$$\boldsymbol{R}_{mn} \exp(i\gamma_{mn}) = (C_{mn} + iQ_{mn})(C_{mm} C_{nn})^{-\frac{1}{2}}. \tag{3.3}$$

The simplest geometry involves horizontal separation of moored instruments (MH). Here the record is the poorest of all. There are no substantial reports of coherence for separations exceeding 10 km; the remaining results available to us are summarized in Table III in order of diminishing horizontal separation X. The first column refers to our analysis of the longshore current component (towards 320°) measured 2 m above bottom with two freely-dropped Snodgrass capsules (Munk, Snodgrass and Wimbush, 1970). The result is not definitive, as the coherence might be associated with poorly resolved tidal lines (record lengths exceeding two months are required for adequate resolution). The close proximity to the sea bottom may be another source of difficulty. Webster (1968a) obtained coherence $\boldsymbol{R}(\omega_i) = 0.67$ between a current meter at 88 m depth at one location, and 98 ± 10 m. at a second location† about 3 km westward. Krauss (1969) obtained poor coherences (qualitative) at inertial and higher frequencies for comparable separations. In the northern North Sea, Schott (1971) measured coherences in a triangular array for currents and temperature (we use the latter). Ufford (1947) employed three vessels from which bathythermograph lowerings were made at intervals of two minutes (!). Our qualitative estimate is based on an inspection of his Figures 5 and 6. Finally Zalkan (1970) used a three-element horizontal array

† The absence of a surface float makes the precise depth uncertain and subject to some time variation.

TABLE III

Moored horizontal (MH) coherence. T is the length of record, h ocean depth, d thermocline depth, and y instrument depth. $\omega_{\frac{1}{2}}$ is the coherence frequency, defined by $\boldsymbol{R}(\omega_{\frac{1}{2}}) = \frac{1}{2}$ (not $\boldsymbol{R}^2 = \frac{1}{2}$) for horizontal separation X. All estimates of $\omega_{\frac{1}{2}}$ are very rough.

	G & M	*Webster*	*Krauss*	*Schott*	*Ufford*	*Zalkan*
	←——Current Meters——→			←——Temperature Probes——→		
	California	W. North Atl.	Baltic	North Sea	California	California
	32°13′N	39°20′N	58°N	56°20′N		30°N
	120°51′W	70°00′W	20°E	1°00′E		121°W
T	10 days	43 days	~ 30 days	12 days	3 hours	20 hours
h	3690 m	2640 m	100 m	82 m		3900 m
d		50 m		32 m	20 m	40 m
y	2 m off bottom	90 m	8, 12, 18, 20 m	32 m	20 m	65 m
X	4 km	3 km	3.4 km, 2.2 km	2.5 km	300 m	30 m
$\omega_{\frac{1}{2}}$	~ 0.14 cph	~ 0.06 cph	poor	0.2 cph	~ 1 cph	8 cph

of automated isotherm followers, suspended from booms mounted on FLIP. With a similar arrangement, Pinkel (personal communication) obtained significant coherence up to 5–8 cph. All coherence estimates are very rough, hardly more than guesses.

The situation is better with regard to MV coherence, thanks largely to the work of Fofonoff and Webster. Their observations at site "D" cover vertical separations from 1 m to 1500 m, at mean depths up to 1600 m. In general $\boldsymbol{R}_{MV}(\omega, Y)$ exceeds 0.7 at inertial frequencies, and drops off at high frequencies. Defining the "half-coherence frequency" $\omega_{\frac{1}{2}}(Y)$ by $\boldsymbol{R}(\omega_{\frac{1}{2}}, Y) = \frac{1}{2}$ (not $\boldsymbol{R}^2 = \frac{1}{2}$), Webster (1971) found that he could obtain a reasonable fit with (Figure 5)

$$(\omega Y)_{\frac{1}{2}} = 13 \text{ cph.m.} \tag{3.4}$$

Siedler's (1971) analysis of currents at site "D" for separations of 4 m to 8 m at depths of about 100 m are also shown. His temperature coherences are much lower (not shown). Perkins (1970) has obtained coherences of 0.6 to 0.7 at the inertial frequency for 500 m vertical separation at various depths (see Table I). Using $\hat{n} = 1.1$ cph, $\hat{\omega}_i = 0.052$ cph gives the plotted point. Coherence between temperature fluctuations at 150 m and at greater depths

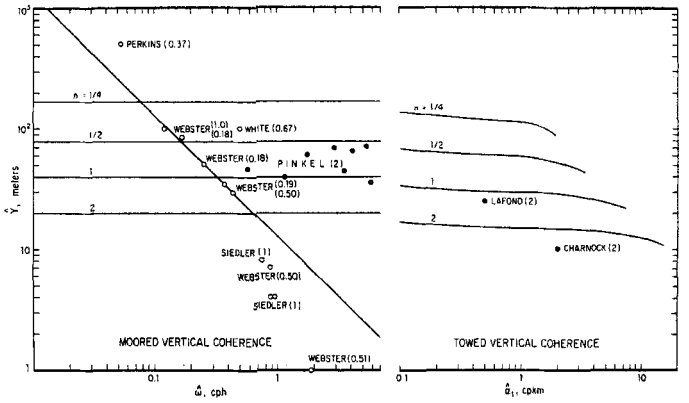

FIGURE 5 The vertical separation $\hat{Y}$ at half-coherence: $\boldsymbol{R}(\hat{Y}, \omega) = \frac{1}{2}$ at left, $\boldsymbol{R}(\hat{Y}, \hat{\alpha}_1) = \frac{1}{2}$ at right (not $\boldsymbol{R}^2 = \frac{1}{2}$). The number ( ) following the name of the investigator is the local Väisälä frequency n (dimensionless). Solid points (due to Pinkel, left; LaFond and Charnock, right) are presumably not subject to fine-structure noise. The 45° line is Webster's rule (3.4), ascribed to fine-structure in §7. The other lines are the theoretical band-limited coherences (§6) at stated values of n.

in the North Atlantic were computed by White (1967). Using his station B (29°N, 18°W, duration 7 days, $d = 100$ m, $h = 2160$ m), the coherences between 150 m and greater depth do not vary systematically with frequency. A representative point (Figure 5) is $\hat{\omega} = 0.5$ cph, $\hat{Y} = 100$ m, $\hat{n} = 2$ cph. Pinkel (personal communication) has computed the coherence between depths of specified isotherms, using repeated temperature soundings from FLIP. Again there is no consistent trend with frequency.

With regard to TV coherence, there are some estimates from Charnock (personal communication) for 10 m vertical separation, and from LaFond for 25 m separation (see Table II for pertinent parameters). The points in Figure 5 can serve for order-of-magnitude orientation only.

4. The equivalent continuum

Perhaps the simplest situation to visualize is that all internal wave energy is concentrated in a single mode. Such a model with mode number $j = \boldsymbol{0}(10)$ can be made to fit the moored and towed spectra (§6) and this may account for Kamenkovich's suggestion (personal communication) that the polygon 2 observations (Kitaigorodsky *et al.*, 1970) are in good accord with an isotropic internal wave field dominated by a single grave mode. However, the single mode fails, and fails completely, to account for the observed lack of coherence between stations separated by a few tens or hundreds of meters vertically. In general terms, the vertical coherence distance (when not affected by fine-structure, §7) is of the order of the reciprocal bandwidth, $Y = \boldsymbol{0}(\Delta\beta)^{-1}$

(Munk and Phillips, 1968), and so infinite for a single discrete mode. Nor is the wavenumber separation between *adjacent* modes an adequate explanation for the low coherence. We need to go to a many-mode model, as has been evident for some time from attempts to fit simultaneous measurements at various depths to superpositions of internal wave modes (Cox and Sandstrom, 1962). At this stage of complexity we prefer to blur the discrete lines into an "equivalent continuum", and replace the strict requirement for standing waves between fixed boundaries with the Tijuana boundary condition: topless and bottom less (M. Rosenbluth, personal communication).

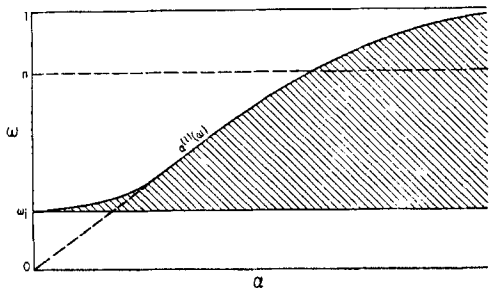

FIGURE 6 Significant contributions to the spectrum at a depth y are confined to the shaded region below $n(y)$.

Solutions are limited by rotation to frequencies above ω_i, and there are no solutions for wavenumbers smaller than that of the gravest mode, $\alpha = \alpha^{(1)}(\omega)$. We thus assume that the significant contributions to the internal wave spectrum come from the shaded region of Figure 6. Further, at a depth y there is no significant contribution to any spectrum from solutions with frequencies greater than $n = e^{-y}$, as such solutions would be below their turning depth and thus negligibly small.

Isotropy

We can further simplify matters by assuming horizontal isotropy throughout. The case for isotropy is conflicting. Relatively strong resonant interaction of internal wave triads (Phillips, 1966, p. 178; Martin *et al.*, 1969) would lead us to expect isotropy, given sufficient time. Spectra of components u_1, u_2 of horizontal currents, measured at moored stations, are generally within a few db's (Fofonoff, 1969b) and the coherence between u_1 and u_2 (§2.8) falls off with frequency (Fofonoff, 1969a); but these are indications of isotropy only at high frequencies, because at inertial frequencies (where most of the energy is concentrated) there is equipartition ($U_L = U_T$) and coherence regardless of the isotropy of the wave field. The *towed* measurements of Charnock (1965) and LaFond and LaFond (1971) are not sensitive to the ship's course, thus indicating isotropy. The towed "polygon traverses" (Kitaigorodsky *et al.*,

1970) suggest anisotropy at the first polygon station, and isotropy at the second polygon. Zalkan (1970), using the triangular array from FLIP, reports a directional event at high frequencies, and suggests a seamount 70 miles distant as a possible source. Voorhis and Perkins (1966) present some evidence for directionality, but the differences in intensity for different directions of tow are not striking.

Energy Integrals

Let $\hat{\rho}\hat{E}(y)$ and $\hat{\rho}\hat{E}$ designate the energy per unit volume and per unit surface area, respectively. Then $\hat{E} = \int_0^{\hat{h}} \hat{E}(y)\, d\hat{y}$, $\hat{y} = \hat{b}y$. The velocity scale is $\hat{M}^{-1}\hat{N}$, and so

$$\hat{E}(y) = \hat{M}^{-2}\hat{N}^2 E(y), \qquad \hat{E} = \hat{M}^{-2}\hat{N}^2\hat{b}E = (2\pi)^{-1}\hat{M}^{-3}\hat{N}^2 E \tag{4.1}$$

defines the dimensionless quantities $E(y)$ and $E = \int_0^h E(y)\, dy$, and draws attention to the fact that *cyclical* wavenumbers (as here used) are scaled with $\hat{M}$, whereas distances (and reciprocal *circular* wavenumbers) are scaled with $\hat{b} = (2\pi\hat{M})^{-1}$.

We now write $\hat{\rho}\hat{E}(\alpha_1, \alpha_2, \omega) = \hat{\rho}\hat{M}^{-4}\hat{N}\hat{b}E(\alpha_1, \alpha_2, \omega)$, for the spectral energy *density* of the equivalent continuum, hence $\iiint E(\alpha_1, \alpha_2, \omega)\, d\alpha_1\, d\alpha_2\, d\omega = E$. The spectrum is confined to a volume generated by rotating the shaded region of Figure 6 about the ω-axis. The mean-square quantities at depth y are given by

$$(\overline{\hat{u}^2}, \overline{\hat{v}^2}, \overline{\hat{\zeta}^2}) = \hat{b}^{-1} \iiint (\overline{U^2}, \overline{V^2}, (2\pi\hat{N})^{-2}\overline{Z^2})\hat{E}(\alpha_1, \alpha_2, \omega)\, d\hat{\alpha}_1\, d\hat{\alpha}_2\, d\hat{\omega}, \tag{4.2}$$

using the average values for the wave functions (2.10, 2.13) as seems appropriate for the equivalent continuum. For horizontal isotropy we may introduce the two-dimensional energy density

$$E(\alpha, \omega) = \int_{-\pi}^{\pi} E(\alpha_1, \alpha_2, \omega)\alpha d\phi = 2\pi\alpha E(\alpha_1, \alpha_2, \omega). \tag{4.3}$$

so that $\iint E(\alpha, \omega)\, d\alpha\, d\omega = E$. (According to our assumption, $E(\alpha, \omega) = 0$ for $\alpha < \alpha^{(1)}(\omega)$.) The mean-square quantities are then given by

$$(\overline{\hat{u}^2}, \overline{\hat{v}^2}, \overline{\hat{\zeta}^2}) = \hat{M}^{-2}\hat{N}^2 \iint (\overline{U^2}, \overline{V^2}, (2\pi\hat{N})^{-2}\overline{Z^2})E(\alpha, \omega)\, d\alpha\, d\omega. \tag{4.4}$$

The energy per unit volume can now be written

$$\left.\begin{aligned} \hat{E}(y) &= \tfrac{1}{2}(\overline{\hat{u}^2} + \overline{\hat{v}^2}) + \tfrac{1}{2}(2\pi\hat{n})^2\overline{\hat{\zeta}^2} = \hat{M}^{-2}\hat{N}^2 \iint \bar{\Phi}(\omega, y)E(\alpha, \omega)\, d\alpha\, d\omega \\ \Phi &= \tfrac{1}{2}(\overline{U^2} + \overline{V^2}) + \tfrac{1}{2}n^2\overline{Z^2} \\ &= n + \tfrac{1}{2}n^{-1}(\omega^2 - \omega_i^2) \quad \text{for} \quad \omega < n; \quad \bar{\Phi} = 0 \quad \text{for} \quad \omega < n. \end{aligned}\right\} \tag{4.5}$$

Equation (4.5) and the normalization condition (2.2, 2.14) are then consistent with (4.1).

The spectrum $E(\alpha, \omega)$ is determined by excitation processes, nonlinear coupling between waves, and dissipation. These processes and their relationships to each other are not yet sufficiently well understood for a theoretical prediction of $E(\alpha, \omega)$ to be possible. Observationally $E(\alpha, \omega)$ will not be known until measurements with suitable arrays of instruments are made. In the meantime we shall attempt to find some form of $E(\alpha, \omega)$ that is at least consistent with known physical and observational constraints.

Moored and Towed Spectra

The moored spectra $F(\omega)$ of velocity and displacement at depth y, defined by

$$\int \hat{F}_{u,v,\zeta}(\omega)\, d\hat{\omega} = [\overline{\hat{u}^2}(y), \overline{\hat{v}^2}(y), \overline{\hat{\zeta}^2}(y)], \tag{4.6}$$

are expressed in terms of the energy spectrum as follows:

$$\hat{F}_{u,v,\zeta}(\omega) = \hat{M}^{-2}\hat{N}[\overline{U^2}, \overline{V^2}, (2\pi\hat{N})^{-2}\overline{Z^2}] \int_0^\infty E(\alpha, \omega)\, d\alpha. \tag{4.7}$$

Measurement of vertical displacement from a horizontal tow in the x_1-direction at a speed S fast compared to the horizontal phase velocity ω/α_1, yields the wavenumber spectrum

$$\hat{F}_\zeta(\alpha_1) = (2\pi)^{-2}\hat{M}^{-3} \int_{\omega_i}^1 d\omega \overline{Z^2} \int_{-\infty}^\infty d\alpha_2 [E(\alpha_1, \alpha_2, \omega) + E(-\alpha_1, \alpha_2, \omega)], \tag{4.8}$$

$\alpha_1 S$ being the frequency of encounter. This corresponds to a projection onto the α_1-axis (not the α-axis). For isotropy the second integral is written $2\int_0^\infty \ldots [2E(\alpha_1, \alpha_2, \omega)]\, d\alpha_2$, there being equal contributions from $\pm\alpha_2$ and from $E(\pm\alpha_1, \alpha_2, \omega)$. Using (4.3) and $\alpha_2^2 = \alpha^2(\omega) - \alpha_1^2$, the towed spectrum then becomes

$$\hat{F}_\zeta(\alpha_1) = \tfrac{1}{2}\pi^{-3}\hat{M}^{-3} \int_{\omega_i}^1 d\omega \overline{Z^2} \int_{\alpha_1}^\infty d\alpha (\alpha^2 - \alpha_1^2)^{-\frac{1}{2}} E(\alpha, \omega). \tag{4.9}$$

(It is understood that $\overline{Z} = 0$ for $\omega > n$ and $E(\alpha, \omega) = 0$ for $\alpha < \alpha^{(1)}(\omega)$.) Thus the towed spectrum at a wavenumber α_1 involves the entire shaded area of α, ω-space (Figure 6) below $\omega = n$ and to the right of α_1, contributions from wavenumbers near α_1 being favored by a factor $(\alpha^2 - \alpha_1^2)^{-\frac{1}{2}}$.

5. Coherence and bandwidth

We express a time series $f(t)$ as a superposition of elementary wave trains of the form

$$\text{Re}\,[g(y) \exp i(\alpha_1 x_1 + \alpha_2 x_2 - \omega t - \varepsilon)], \tag{5.1}$$

where ε is the phase, assumed to be random, and $g(y)$ is the appropriate component of the wave functions

$$\begin{bmatrix} i\,U_L(y)\cos\phi - U_T(y)\sin\phi \\ i\,U_L(y)\sin\phi + U_T(y)\cos\phi \\ V(y) \\ i\,Z(y) \end{bmatrix} \tag{5.2}$$

from (1.2) with U_L, U_T, V, Z given by (2.1). We then have (Eq. 3.2)

$$C_{mn}(\omega) + i\,Q_{mn}(\omega) = \int_{-\infty}^{\infty} d\alpha_1 \int_{-\infty}^{\infty} d\alpha_2 E(\alpha_1, \alpha_2, \omega) g^*(\omega, y_m) g_n(\omega, y_n) \times \exp i(\alpha_1 X_1 + \alpha_2 X_2) \tag{5.3}$$

for the co- and quadrature spectra between time series at moored stations, where $E(\alpha_1, \alpha_2, \omega)$ is the spectral energy density (§4) and the vector $(X_1, X_2, y_n - y_m) = \boldsymbol{r}_n - \boldsymbol{r}_m$. Similar formulae apply for the co- and quadrature spectra between time series from different towed instruments (see later). We see that (5.3) does reduce to the moored spectra when $m = n$, assuming isotropy and using the mean values for the squared wave functions. Horizontal *separations* (but vertical *positions*) appear in (5.3) as a result of the assumed horizontal (but not vertical) stationarity.

Moored Component (MC) Coherence

The co- and quadrature spectra of the two components u_1, u_2 of horizontal current measured at the same position are given by

$$C_{12}(\omega) + i\,Q_{12}(\omega) = \int_0^{\infty} d\alpha \int_0^{2\pi} \alpha\, d\phi\; E(\alpha_1, \alpha_2, \omega)[(U_L^2 - U_T^2)\cos\phi \sin\phi - i\,U_L U_T] \tag{5.4}$$

using the suffices 1, 2 to refer to the two components. For an isotropic energy distribution, with $E(\alpha_1, \alpha_2, \omega) = (2\pi\alpha)^{-1} E(\alpha, \omega)$,

$$C_{12} + i\,Q_{12} = -i \int_0^{\infty} U_L U_T E(\alpha, \omega)\, d\alpha, \quad C_{11} = C_{22} = \int_0^{\infty} \tfrac{1}{2} U^2 E(\alpha, \omega)\, d\alpha \tag{5.5}$$

(the factor $\frac{1}{2}$ enters as $\overline{u_1^2} = \overline{u_2^2} = \frac{1}{2}\overline{u^2}$ (Eq. 2.13)). The r.m.s. values of U_L, U_T, U (Eq. 2.10, 13) are independent of α, but U_L, U_T are of opposite sign (Eq. 2.1) and we obtain simply

$$\boldsymbol{R}_{12} = \frac{2\omega\omega_i}{\omega^2 + \omega^2}, \qquad \gamma_{12} = \tfrac{1}{2}\pi. \tag{5.6}$$

Thus u_2 lags u_1 by $\frac{1}{2}\pi$ (clockwise rotation in the northern hemisphere), and the coherence decreases from a value of 1 at the inertial frequency.

Fofonoff (1969a) has investigated the MCC in greater detail on the assumption that the observed currents are due to internal waves behaving as if in a region of constant Väisälä frequency (see end of §2), but without the further assumption of isotropy. He introduces the "collinear" and "rotary" coherences $\boldsymbol{R}_c$ and $\boldsymbol{R}_r$; these are independent of the orientation of the axes and have the property $\boldsymbol{R}_c^2+\boldsymbol{R}_r^2 = \boldsymbol{R}_{12}^2$. $\boldsymbol{R}_c = 0$ for isotropy, and $\boldsymbol{R}_c = (\omega^2-\omega_i^2)/(\omega^2+\omega_i^2)$ for a uni-directional spectrum. Observations are much closer to the former extreme. $\boldsymbol{R}_r = 2\omega\omega_i/(\omega^2+\omega_i^2)$ *generally*, and here agreement with observations supports only the assumption that the fluctuating currents are due to internal waves. We see that for isotropy $\boldsymbol{R}_r = \boldsymbol{R}_{12}$ (as $\boldsymbol{R}_c = 0$), in accord with (5.6).

Moored Horizontal (MH) Coherence

For two stations at the same depth y, separated horizontally by $(X_1, X_2) = (X, 0)$, say, the quadrature spectrum of u_1 at both stations, or of u_2 at both stations, is zero for isotropy, and the co-spectrum is given by

$$C(X,\omega) = \int_0^\infty d\alpha \int_0^{2\pi} \alpha d\phi\, (2\pi\alpha)^{-1} E(\alpha,\omega)\tfrac{1}{2}\overline{U^2}(\omega, y) \exp(i\alpha X\cos\phi), \qquad (5.7)$$

where we have used the mean square value of the wave function. Now $\frac{1}{2}\pi^{-1}\int_0^{2\pi} \exp(i\alpha X\cos\phi)\, d\phi = J_0(\alpha X)$ so that the coherence is

$$\boldsymbol{R}(X,\omega) = \int_0^\infty E(\alpha,\omega)J_0(\alpha X)\, d\alpha / \int_0^\infty E(\alpha,\omega)\, d\alpha \qquad (5.8)$$

and this in fact gives the coherence between any two variables measured at a separation X, though for some pairs the phase is non-zero.

(5.8) is closely related to the Hankel transform of $E(\alpha, \omega)$. The inverse is

$$E(\alpha,\omega) = \left(\int_0^\infty E(\alpha,\omega)\, d\alpha\right) \int_0^\infty \boldsymbol{R}(X,\omega)(\alpha X)J_0(\alpha X)\, dX, \qquad (5.9)$$

so that $E(\alpha, \omega)$ is an undetermined function of ω times a function of α and ω which in principle may be obtained from the coherence.

Moored Vertical (MV) Coherence

The coherence of u_1 (say) for two stations separated vertically, but not horizontally, is somewhat more complicated. The wave functions U_L, U_T are independent of azimuth ϕ, so that, integrating over α for an isotropic energy density,

$$C(\omega)+i\,Q(\omega) = \tfrac{1}{2}\int_0^\infty E(\alpha,\omega)[U_L(y_1)U_L(y_2)+U_T(y_1)U_T(y_2)]\, d\alpha \qquad (5.10)$$

$$= \tfrac{1}{2}n_1n_2(1+\omega_i^2/\omega^2)\int_0^\infty E(\alpha,\omega)J_a'(k_1)J_a'(k_2)N^2(\omega,\alpha)\, d\alpha \qquad (5.11)$$

using (2.1). The r.h.s. is real, thus $Q = 0$ and $\gamma = 0$. The subscripts 1, 2 on y, n, k refer now to the two stations. (2.9, 11) give

$$J_a'(k_1)J_a'(k_2)N^2 = (n_1n_2)^{-\frac{1}{4}}[\cos(k_1-k_2)-\cos(k_1+k_2-2K)] \tag{5.12}$$

where

$$K = (\tfrac{1}{4}+\tfrac{1}{2}a)\pi \quad \text{for} \quad \omega \gg n_h; \qquad K = k_0 \quad \text{for} \quad \omega \ll n_h. \tag{5.13}$$

For a vertical separation $Y = y_2-y_1 \ll 1$ (i.e. $\hat{Y} \ll \hat{b}$) the difference wavenumber

$$k_1-k_2 = a\omega^{-1}(e^{-y_1}-e^{-y_2}) \approx (a\omega^{-1}e^{-y})Y = kY, \quad y = \tfrac{1}{2}(y_1+y_2), \tag{5.14}$$

is small compared to the sum wavenumber k_1+k_2, and so for either case (5.13), and thus presumably for all ω,

$$\boldsymbol{R}(Y, \omega; y) = \int_0^\infty E(\alpha, \omega)\cos kY\, d\alpha \Big/ \int_0^\infty E(\alpha, \omega)\, d\alpha. \tag{5.15}$$

It is surprising that the coefficient of Y is $k = an/\omega$ rather than $\beta = a(n^2-\omega^2)^{\frac{1}{2}}/\omega$ (appropriate for a constant n model). Neither coefficient is accurate near the Väisälä frequency n, but k is preferable (see end of §2).

In deriving (5.15) we have used the normal mode functions, thus assuming standing waves in the vertical. If the wave propagation is entirely upwards (corresponding to energy transmission downwards), (5.15) becomes

$$\boldsymbol{R}\, e^{i\gamma} = \int_0^\infty E(\alpha, \omega)\, e^{-ikY}\, d\alpha \Big/ \int_0^\infty E(\alpha, \omega)\, d\alpha. \tag{5.16}$$

where γ is the phase by which the lower station lags the upper. For a solution made up of two progressive waves of unequal amplitude propagating in opposite directions, the average phase progression is in the same direction and at the same rate as the larger of the two progressive waves. Thus if there is a tendency for waves of all α to have some slight downward energy transmission, (5.16) is the appropriate formula for the coherence and phase (with $-i$ replaced by i for energy transmission upwards). If on the other hand some values of α have upward and some downward energy transmission, (5.15) is more appropriate. In any case, the magnitude of $\boldsymbol{R}$ is little affected.

The inverse transform of (5.15) is (using $\alpha = a(1-\omega_i^2/\omega^2)^{\frac{1}{2}}$)

$$E(\alpha, \omega) = \left(\int_0^\infty E(\alpha, \omega)\, d\alpha\right)\frac{1}{2\pi}\int_0^\infty \boldsymbol{R}(Y, \omega; y)n(y)(\omega^2-\omega_i^2)^{-\frac{1}{4}}\cos kY\, dY \tag{5.17}$$

so that, as before, $E(\alpha, \omega)$ may be determined from the coherence to within an unknown function of ω. A similar formula applies for the inverse of (5.16).

TOWED VERTICAL (TV) COHERENCE

The coherence between measurements of vertical displacement by two horizontally towed instruments, separated by a vertical distance Y, is derived in a similar manner to the MV coherence and the towed spectrum (4.9). If there is no net vertical energy propagation,

$$\boldsymbol{R}(Y, \alpha_1; y) = \frac{\int_{\omega_i}^{n} d\omega \int_{\alpha_1}^{\infty} (\alpha^2 - \alpha_1^2)^{-\frac{1}{2}} E(\alpha, \omega) \overline{Z^2}(\omega, y) \cos kY \, d\alpha}{\int_{\omega_i}^{n} d\omega \int_{\alpha_1}^{\infty} (\alpha^2 - \alpha_1^2)^{-\frac{1}{2}} E(\alpha, \omega) \overline{Z^2}(\omega, y) \, d\alpha}. \quad (5.18)$$

As for the MV coherence, $\cos kY$ is replaced by $e^{\pm ikY}$ for upward or downward energy propagation.

6. Energy distribution in α, ω-space

THE EQUIMODAL SPECTRUM

Let us first consider the form of $E(\alpha, \omega)$ on the assumption that all modes are equally excited. For a given ω, $E(\alpha_1, \alpha_2, \omega)$ is then inversely proportional to $\delta\alpha$, the distance between modal surfaces, and so $E(\alpha, \omega) \propto \alpha/\delta\alpha$. Likewise, for a given α, $E(\alpha, \omega) \propto 1/\delta\omega$. For $\omega < 0.2$ or so, an adequate approximation to the dispersion relation is $\alpha^2 = j^2\pi^2(\omega^2 - \omega_i^2)$. Hence

$$\delta\alpha \propto (\omega^2 - \omega_i^2)^{\frac{1}{2}}, \qquad \delta\omega \propto \alpha^{-1}\omega^{-1}(\omega^2 - \omega_i^2)^{\frac{1}{2}}. \quad (6.1)$$

Thus for fixed ω, $E(\alpha, \omega) \propto \alpha$, and for fixed α, $E(\alpha, \omega) \propto \omega(\omega^2 - \omega_i^2)^{-\frac{1}{2}}$. Accordingly the "equimodal spectrum" is

$$E_m(\alpha, \omega) \propto \alpha\omega(\omega^2 - \omega_i^2)^{-\frac{1}{2}}. \quad (6.2)$$

The integrated energy clearly diverges, as of course it must for an infinity of modes. However, the form of (6.2) does suggest a weaker dependence of $E(\alpha, \omega)$ on $(\omega^2 - \omega_i^2)$.

A CONVENIENT REPRESENTATION

Any separated form $E(\alpha, \omega) = A(\alpha) \cdot \Omega(\omega)$ is incompatible with the observations of MV coherence (§5), which indicate that the α-bandwidth is a function of frequency, $\mu(\omega)$, say. We make the *similarity* assumption that the *scale* of $E(\alpha, \omega)$ as a function of α is proportional to μ; but that its *shape* is invariable:

$$E(\alpha, \omega) = c\mu^{-1}A(\lambda)\Omega(\omega), \qquad \lambda = \alpha/\mu \quad (6.3)$$

where $A(\lambda) = 0$ for $\lambda < \lambda^{(1)} = \alpha^{(1)}/\mu$. $\lambda^{(1)}$ is sufficiently small that for most purposes it may be taken as zero.

Without loss of generality we impose the condition

$$\int_0^\infty A(\lambda)\, d\lambda = 1, \tag{6.4}$$

so that

$$\int_0^\infty E(\alpha, \omega)\, d\alpha = c\Omega(\omega), \qquad E = c\int_{\omega_i}^1 \Omega(\omega)\, d\omega, \tag{6.5}$$

thus expressing the constant c in terms of the energy E (Eq. 4.5).

Choosing $\Omega(\omega)$ to fit the moored spectrum The simplest form of $\Omega(\omega)$ would be a power law. However, in view of the form (6.2) of the equimodal spectrum, and the cusp at ω_i in the moored current spectra (§3), we take

$$\Omega(\omega) = \omega^{-p+2s}(\omega^2 - \omega_i^2)^{-s} \tag{6.6}$$

which becomes ω^{-p} away from ω_i. For the moored current spectra to cusp at ω_i, but with $\int_{\omega_i}^1 \Omega(\omega)\, d\omega$ finite, we require $0 < s < 1$. We arbitrarily choose the mid-point, $s = \frac{1}{2}$. From (4.7) the moored spectra at depth y are

$$\hat{F}_{u,\zeta}(\omega) = \hat{M}^{-2}\hat{N}c\omega^{-p-1}[n(\omega^2+\omega_i^2)(\omega^2-\omega_i^2)^{-\frac{1}{2}}, \quad (2\pi\hat{N})^{-2}n^{-1}(\omega^2-\omega_i^2)^{\frac{1}{2}}] \tag{6.7}$$

$$= \hat{M}^{-2}c\omega^{-p}\left[\hat{n}, \frac{1}{4\pi^2\hat{n}}\right] \quad \text{for} \quad \omega \gg \omega_i. \tag{6.8}$$

Most of the contribution to the mean-square quantities comes from near the inertial frequencies, and so for $p = 2$ (as suggested by the observed spectra)

$$[\overline{\hat{u}^2}, \overline{\hat{\zeta}^2}] \approx \int_{\omega_i}^\infty \hat{F}_{u,\zeta}(\omega)\, d\hat{\omega} = \left[\tfrac{3}{2}\hat{n}, \frac{1}{8\pi^2\hat{n}}\right]\hat{M}^{-2}\hat{N}E, \qquad c = \frac{2\omega_i E}{\pi} \tag{6.9}$$

Choosing $A(\lambda)$ to fit the towed spectrum The simplest form for $A(\lambda)$ is

$$A(\lambda) = 1 \quad \text{for} \quad 0 \leqq \lambda \leqq 1, \qquad A(\lambda) = 0 \quad \text{for} \quad \lambda > 1, \tag{6.10}$$

consisting of a plateau terminated by a cliff. We have considered more general models, with SLOPE regions beyond gently sloping HIGHLANDS (Figure 7), but these models lead either to inconsistencies with the data (particularly the TV coherence) or to results essentially the same as for (6.10).

The energy spectrum is now

$$E(\alpha, \omega) = c\mu^{-1}\omega^{-p+1}(\omega^2-\omega_i^2)^{-\frac{1}{2}} \quad \text{for} \quad \alpha^{(1)}(\omega) \leqq \alpha \leqq \mu \tag{6.11}$$

and zero otherwise, so that from (4.9)

$$\hat{F}_\zeta(\alpha_1) = \tfrac{1}{2}c\hat{M}^{-3}\pi^{-3}n^{-1}\int_{\omega_\mu}^n d\omega\, (\omega^2-\omega_i^2)^{\frac{1}{2}}\omega^{-p-1}\mu^{-1}\int_{\alpha_1}^\mu (\alpha^2-\alpha_1^2)^{-\frac{1}{2}}\, d\alpha, \tag{6.12}$$

defining ω_μ by $\mu(\omega_\mu) = \alpha_1$ (Figure 7). The lower limit of the α-integration should really be $\max(\alpha^{(1)}, \alpha_1)$, but this makes little difference except for very small α_1. Clearly $\hat{F}_\zeta(\alpha_1) = 0$ for $\alpha_1 \geqq \mu(n)$.

For further progress we need to specify $\mu(\omega)$. By analogy with (6.6) we consider the form

$$\mu = j_i\pi(\omega/\omega_i)^{r-1}(\omega^2-\omega_i^2)^{\frac{1}{2}} \tag{6.13}$$

so that j_i is the equivalent number of modes at the inertial frequency (Eq. 1.6).

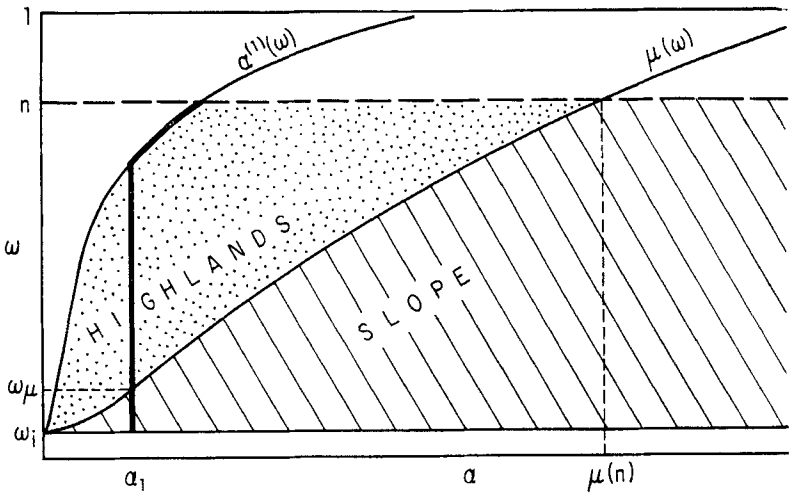

FIGURE 7 The spectrum at a depth y is confined to the area between ω_i and $n(y)$ to the right of $\alpha^{(1)}(\omega)$, but the unshaded region to the left of $\alpha^{(1)}(\omega)$ is so narrow that its existence can ordinarily be ignored ($\alpha^{(1)}(\omega)$ is exaggerated relative to $\mu(\omega)$ in the above schematic). In our simplified model the HIGHLANDS are flat, terminated by a cliff at $\mu(\omega)$. The towed spectra and TV coherence are associated with the region to the right of the heavy line, and for $\alpha_1 > \mu(n)$ involve only the SLOPE area (which vanishes in our cliff model).

Now $\omega_\mu \gg \omega_i$ except for very small α_1. Moreover, the ω-integrand decreases rapidly with increasing ω, so that we may replace the upper limit n by ∞ provided $\omega_\mu \ll n$; using a dummy variable $x = j_i\pi(\omega/\omega_i)^r\alpha_1^{-1}$ the integration can be carried out, and gives

$$\hat{F}_\zeta(\alpha_1) \approx c\hat{M}^{-3}n^{-1}\alpha_1^{-q}\frac{[j_i\pi/\omega_i^r]^{q-1}\Gamma[\frac{1}{2}q]}{4\pi^{\frac{1}{2}}qr\Gamma[\frac{1}{2}(q+1)]} \tag{6.14}$$

provided $\omega_i \ll \omega_\mu \ll n$ with $\mu(\omega_\mu) = \alpha_1$, defining

$$q = (p+r-1)/r, \quad \text{i.e.} \quad r = (p-1)/(q-1). \tag{6.15}$$

Thus the exponents p, q in the power laws (when $\omega \gg \omega_i$) for the moored and towed spectra determine the power law for the α-bandwidth, $\mu \propto \omega^r$. The relation (6.15) is more general than the conditions for which it has here been derived; for example, it holds for any model satisfying the similarity assumption leading to (6.3).

Moored vertical coherence According to (5.15)

$$\boldsymbol{R}_{\mathrm{MV}}(Y, \omega; y) = \int_0^\infty A(\lambda) \cos \lambda B \, d\lambda, \qquad B = \mu n Y(\omega^2 - \omega_i^2)^{-\frac{1}{2}}. \quad (6.16)$$

$\boldsymbol{R}_{\mathrm{MV}} = 1$ for $B = 0$, and decreases with increasing B, reaching a value $\boldsymbol{R}_{\mathrm{MV}} = \frac{1}{2}$ for $B = 1.9$, hence $(\mu\omega^{-1} n Y)_{\frac{1}{2}} = 1.9$ for $\omega \gg \omega_i$. Webster's rule (Eq. 3.4), $(\omega Y)_{\frac{1}{2}} =$ constant, implies $\mu \propto \omega^2$ away from ω_i and hence $r = 2$.

Incompatibility

Some relevant sets of values of p, q, r (Eq. 6.15) are given below:

Exponent p in $F_u(\omega) \propto \omega^{-p}$	5/3	5/3	2	2	2	3
q in $F_\zeta(\alpha_1) \propto \alpha_1^{-q}$	5/3	2	3/2	5/3	2	2
r in $\mu \propto \omega^r$	1	2/3	2	3/2	1	2

The observed spectra indicate $p = q = 2$, though the more fashionable 5/3 is often claimed.† Values of p and q between 5/3 and 2 yield r between 2/3 and 3/2, incompatible with Webster's rule. Our resolution of this difficulty is to attribute Webster's rule to the effects of oceanic fine-structure rather than bandwidth (see §7), and to choose the integer components

$$(p, q, r) = (2, 2, 1). \quad (6.17)$$

The Proposed Spectrum

We now write

$$E(\alpha, \omega) = E(2/\pi)\omega_i \mu^{-1} \omega^{-1} (\omega^2 - \omega_i^2)^{-\frac{1}{2}}, \quad \alpha^{(1)} \leqq \alpha \leqq \mu, \quad (6.18)$$

with

$$\mu(\omega) = j_i \pi (\omega^2 - \omega_i^2)^{\frac{1}{2}}. \quad (6.19)$$

† Turbulence not dominated by buoyancy takes over at higher wavenumbers than we have here discussed; an upper length limit is the Richardson scale $(\hat{\varepsilon}/\hat{n}^3)^{\frac{1}{2}}$, which is $O(1\text{ m})$ for a dissipation $\hat{\varepsilon} = 10^{-4}\,\mathrm{cm^2\,sec^{-3}}$. Viscous effects are significant at scales less than $O(\hat{\nu}/\hat{n})^{\frac{1}{2}} = 0.5\,\mathrm{cm}$.

This gives $\hat{E}(y) \approx \hat{M}^{-2}\hat{N}^2 nE$ (Eq. 4.5), and

$$\left.\begin{aligned} \hat{n}^{-1}\hat{F}_u(\omega) &= 2\pi^{-1}E\omega_i\hat{M}^{-2}\omega^{-3}(\omega^2+\omega_i^2)(\omega^2-\omega_i^2)^{-\frac{1}{2}}, \\ \hat{n}\hat{F}_\zeta(\omega) &= \tfrac{1}{2}\pi^{-3}E\omega_i\hat{M}^{-2}\omega^{-3}(\omega^2-\omega_i^2)^{\frac{1}{2}} \end{aligned}\right\} \tag{6.20}$$

$$\hat{n}\hat{F}_\zeta(\alpha_1) = j_i^{-1}\pi^{-5}E\omega_i\hat{M}^{-3}\hat{N}\int_{\omega_\mu}^{n}\omega^{-3}\cosh^{-1}(\mu/\alpha_1)\,d\omega \tag{6.21}$$

$$\approx \tfrac{1}{2}j_i\pi^{-3}E\omega_i\hat{M}^{-3}\hat{N}\alpha_1^{-2} \quad \text{for} \quad \omega_i \ll \omega_\mu \ll n. \tag{6.22}$$

For very small α_1 we must allow for the mode 1 cut-off of $E(\alpha, \omega)$. In the limit $\alpha_1 = 0$ the integral in (6.21) is replaced by $\int_{\omega_i}^{n}\omega^{-3}\ln(\mu/\alpha^{(1)})\,d\omega \approx 1.5\,\omega_i^{-2}$ for the case $j_i = 20$, so that

$$\hat{n}\hat{F}_\zeta(0) = 0.08\pi^{-5}E\omega_i^{-1}\hat{M}^{-3}\hat{N} \quad \text{for} \quad j_i = 20. \tag{6.23}$$

Numerical integration then yields $\hat{F}_\zeta(\alpha_1) = \frac{1}{2}\hat{F}_\zeta(0)$ for $\hat{\alpha}_1 = 0.04$ cpkm.

Curve fitting The moored and towed spectra (the latter numerically evaluated) have been plotted in Figure 4 for

$$j_i = 20, \quad E = 2\pi\times 10^{-5}, \quad \hat{\rho}\hat{E} = 0.382 \text{ joules cm}^{-2} \tag{6.24}$$

(using $\hat{M}^{-3}\hat{N}^2 = 3.82\times 10^{11}$ cm^3 sec^{-2}).† With this choice of constants we can fit both the moored and towed spectra at the low frequencies (wavenumbers), thus indicating some degree of universality. The computed buoyancy cut-off, whether abrupt as is the case for frequency, or tapered as is the case for wavenumber, is evident only in the Voorhis spectrum and also possibly in Gould's (1971) spectrum. This discrepancy will be attributed to fine-structure (§7). It is perhaps significant that the Voorhis spectra are not subject to fine-structure.

Equivalent single mode An equivalent analysis (not given) for the case that all energy is concentrated in some single mode leads to the same expression (6.20) for $F_u(\omega)$, and agrees with the result (6.22) for $F_\zeta(\alpha_1)$ provided the single mode number is $\frac{1}{2}j_i(= 10)$. The single mode model is of course entirely inadequate for any insight into the coherence problem.

Coherence For the proposed spectrum the MH coherence (5.8) reduces to

$$R_{\text{MH}}(X, \omega) = \int_0^1 J_0(\lambda\mu X)\,d\lambda \tag{6.25}$$

† For comparison, the energy in surface tides is about 0.3 joules cm^{-2} (Hendershott, 1971); for one deep station off San Diego, Cox (1966) has estimated an internal tide energy one-third the surface tide energy. Munk and Phillips (1968) have estimated $j_i = O(10)$ from the observed "blue shift" of the inertial peak.

which reaches a value $\frac{1}{2}$ for $\mu X = 2.8$, hence

$$R_{MH} = \tfrac{1}{2} \quad \text{for} \quad \hat{X}_{\frac{1}{2}} = 58\,(\omega^2 - \omega_i^2)^{-\frac{1}{2}} \text{ meters.} \tag{6.26}$$

The infinity in $X_{\frac{1}{2}}$ at ω_i is presumably removed by the finite resolution imposed by a finite record length, and by other considerations not in our model (Munk and Phillips, 1968). Away from ω_i, the coherence distance varies inversely with frequency, giving $\hat{X}_{\frac{1}{2}} = 2000$, 200, 30 m for $\hat{\omega} = 0.1$, 1, 6 cph, respectively, consistent with the rather limited evidence (Table 3).

The MV coherence drops to $\frac{1}{2}$ for $\mu n Y(\omega^2 - \omega_i^2)^{-\frac{1}{2}} = 1.9$, hence

$$R_{MV} = \tfrac{1}{2} \quad \text{for} \quad n\hat{Y}_{\frac{1}{2}} = 40 \text{ meters,} \tag{6.27}$$

in rough agreement with Pinkel's data (not subject to fine-structure). Other observations (Figure 5, left) are presumably limited by bandwidth at low frequencies and by fine-structure at high frequencies.

According to (5.18)

$$R_{TV}(Y, \alpha_1) = \int_{\omega_\mu}^{n} d\omega\, \omega^{-3} \mu \int_{\alpha_1}^{\mu} (\alpha^2 - \alpha_1^2)^{-\frac{1}{2}} \cos \lambda B\, d\lambda \Big/ \int_{\omega_\mu}^{n} \omega^{-3} \cosh^{-1}(\mu/\alpha_1)\, d\omega \tag{6.28}$$

$$\approx 2 \int_1^\infty dz\, z^{-3} \int_1^z (x^2 - 1)^{-\frac{1}{2}} \cos(j_i \pi n Y x/z)\, dx \quad \omega_i \ll \omega_\mu \ll n. \tag{6.29}$$

In this range $\omega_i \ll \omega_\mu \ll n$ one obtains

$$R_{TV} = \tfrac{1}{2} \quad \text{for} \quad n\hat{Y}_{\frac{1}{2}} = 30 \text{ meters,} \tag{6.30}$$

in good accord with the measurements of LaFond and Charnock (Figure 5, right). According to the approximation (6.30) $\hat{Y}_{\frac{1}{2}}$ is independent of wavenumber; a numerical integration of (6.28) (Figure 5) shows only a slight wavenumber dependence. On the other hand LaFond and Charnock found a marked decrease of $R_{TV}(Y, \alpha_1)$ with $\hat{\alpha}_1$ between 0.1 and 1 cpkm which implies a decrease of $\hat{Y}_{\frac{1}{2}}$ with increasing $\hat{\alpha}_1$.

7. Fine-structure contamination

Our discussion so far assumes an interpretation of the observations in terms of internal wave solutions for an ocean with smooth vertical variations of its properties. Over the last decade evidence has accumulated (Woods and Fosberry, 1966; Woods, 1968; Stommel and Fedorov, 1967, Cox *et al.*, 1969) that the vertical changes in temperature and salinity are concentrated in thin sheets, separated by thicker layers of fairly homogeneous water. From (1.3) the second derivatives d^2V/dy^2, $d^2\zeta/dy^2$ of the wave-functions for vertical

velocity and displacement are then concentrated at the sheets. Accordingly dV/dy and $d\zeta/dy$ are quasi-discontinuous at the sheets, but the wave-functions $V(y)$ and $\zeta(y)$ themselves are not. Consequently, direct measurement of vertical velocity and displacement can legitimately be compared with internal wave solutions based on the smoothed density profile.

The same does not hold for measurements of temperature and current at a fixed depth. dT/dy and dU/dy are concentrated at the sheets, so that $T(y)$ and $U(y)$ have a step-like structure superposed on the smooth profile that would be observed in the absence of fine-structure. Our concern here is whether this fine-structure "noise" may dominate some of the observed spectra and coherences and thus invalidate the interpretation in terms of the gross internal wave solutions.

The spikes in dT/dy and dU/dy are associated with a "white" fine-structure noise for time series of these gradients, hence σ^{-2}-spectra (frequency or wavenumber) for $T(t)$ or $U(t)$, and σ^{-4} for $V(t)$ or $\zeta(t)$. Phillips (1971) has shown that the bandwidth is determined by the thickness of the layers and of the sheets separating the layers. Garrett and Munk (1971, henceforth GM) have examined the problem in more detail and attempted a comparison of the "fine-structure spectrum" with the basic "gradient spectrum." For a σ^{-2} gradient spectrum (as indicated for moored measurements by Voorhis (1968), and for towed measurements by Charnock (1965) and LaFond and LaFond (1971)) we found that the relative intensity γ of the fine-structure spectrum is sensitive to the largest scale of fine-structure (GM, Eq. (31)), and that γ also determines the overlap in frequency between fine-structure and gradient spectra. Referring to Figure 4, we suggest that the σ^{-2} continuation of the Fofonoff and Ewart spectra beyond the computed buoyancy cut-offs (frequency and wavenumber) is the result of fine-structure, and that the Voorhis cut-off may be the σ^{-4} fine-structure spectrum. The moored spectra (other than Voorhis) may be dominated by fine-structure down to perhaps 0.3 cph. This would call for $\gamma = \mathcal{O}(10)$ and a maximum fine-structure scale of 50 meters. Against this interpretation is the lack of any evidence in the Fofonoff spectra for a transition from the gradient to the fine-structure range, and the fact that Fofonoff intensities are rather less than $\mathcal{O}(10)$ times the Voorhis intensities.

In the frequency band dominated by fine-structure we find (GM, §10) a MV coherence loss due to fine-structure consistent with

$$R_{\mathrm{MV}}(\omega) = \tfrac{1}{2} \quad \text{for} \quad \hat{\omega}\hat{Y} \approx \overline{(\hat{\omega}^2\hat{\zeta}^2)}^{\frac{1}{2}} \tag{7.1}$$

which is of the same form as Webster's rule (3.4), and identifies Webster's empirical constant with a vertical velocity characteristic of the internal waves. More precisely, $\overline{\hat{\zeta}^2} = \int \hat{F}_\zeta(\omega)\, d\hat{\omega}$ and $\hat{\omega}^2 = \int \hat{\omega}^2 \hat{F}_\zeta(\omega)\, d\hat{\omega} / \int \hat{F}_\zeta(\omega)\, d\hat{\omega}$ are the

mean-square vertical displacement and frequency; for the proposed model their product equals

$$\overline{\hat{\omega}^2\hat{\zeta}^2} = \int_{\omega_i}^{n} \hat{\omega}^2\hat{F}_\zeta(\omega)\,d\hat{\omega} = \tfrac{1}{2}\pi^{-3}\hat{N}^2\hat{M}^{-2}n^{-1}E\omega_i \int_{\omega_i}^{n} \omega^{-1}(\omega^2-\omega_i^2)^{\frac{1}{2}}\,d\omega$$
$$= \tfrac{1}{2}\pi^{-3}\hat{N}^2\hat{M}^{-2}E\omega_i(1-\tfrac{1}{2}\pi(\omega_i/n)+\ldots). \tag{7.2}$$

Using $E = 2\pi\times 10^{-5}$ this gives 2.6 cph.m as compared to Webster's 13 cph.m. There are many ways of modifying both of these numbers and so reducing the discrepancy. For the present we are content to be within one order of magnitude, and conclude that the small coherence distances at high frequencies (Figure 5) are the result of fine-structure.

8. Doppler-shifted spectra

For a sensor moving in the positive x_1-direction at a constant speed S we have $x_1 = St$; the observed phase of an elementary wave train $e^{i\gamma}$ is then

$$\gamma = \alpha_1 x_1 + \alpha_2 x_2 - \omega t = \alpha_2 x_2 - (\omega - \alpha_1 S)t. \tag{8.1}$$

The contribution to the frequency-of-encounter

$$\sigma = |\omega - \alpha_1 S| \tag{8.2}$$

comes from three branches (Figure 8):

(i) $\alpha_1 < 0$, $\omega > \alpha_1 S$: "negative" waves (travelling opposite to sensor)

(ii) $\alpha_1 > 0$, $\omega > \alpha_1 S$: positive waves, overtaking the sensor

(iii) $\alpha_1 > 0$, $\omega < \alpha_1 S$: sensor overtaking positive waves

(allowing that ω is always positive). Accordingly

$$\hat{F}_\zeta(\sigma) = \tfrac{1}{4}\pi^{-3}\hat{M}^{-3}\hat{S}^{-1}\int_{\omega_t}^{n} d\omega\,\overline{Z^2}\left\{\int_{|\omega-\sigma|/S}^{\infty}\left[\alpha^2-\left(\frac{\omega-\sigma}{S}\right)^2\right]^{-\frac{1}{2}}E(\alpha,\omega)\,d\alpha\right.$$
$$\left.+\int_{(\omega+\sigma)/S}^{\infty}\left[\alpha^2-\left(\frac{\omega+\sigma}{S}\right)^2\right]^{-\frac{1}{2}}E(\alpha,\omega)\,d\alpha\right\}. \tag{8.3}$$

Here the first integral refers to (i) for $\sigma > \omega$ and to (ii) for $\sigma < \omega$, the second integral refers to (iii). For very fast tows, and accordingly very high recorded σ, the contribution from (ii) disappears, the contributions from (i) and (iii) become nearly identical and (8.3) approaches (4.9) where $\sigma = \alpha_1 S$ and

$\hat{F}_\zeta(\sigma) = \hat{S}^{-1}\hat{F}_\zeta(\alpha_1)$. This problem has been discussed by Voorhis and Perkins (1966).

For slow tows the integration in α, ϕ-space is more convenient; (8.3) can then be written

$$\hat{F}_\zeta(\sigma) = \tfrac{1}{4}\pi^{-3}\hat{M}^{-2}\hat{N}^{-1}\int_0^\pi d\phi \int_0^\infty \overline{Z^2}(\omega, \mathrm{y})E(\alpha, \omega)\, d\alpha \tag{8.4}$$

where

$$\omega(\alpha, \phi) = |\sigma + \alpha S \cos\phi|. \tag{8.5}$$

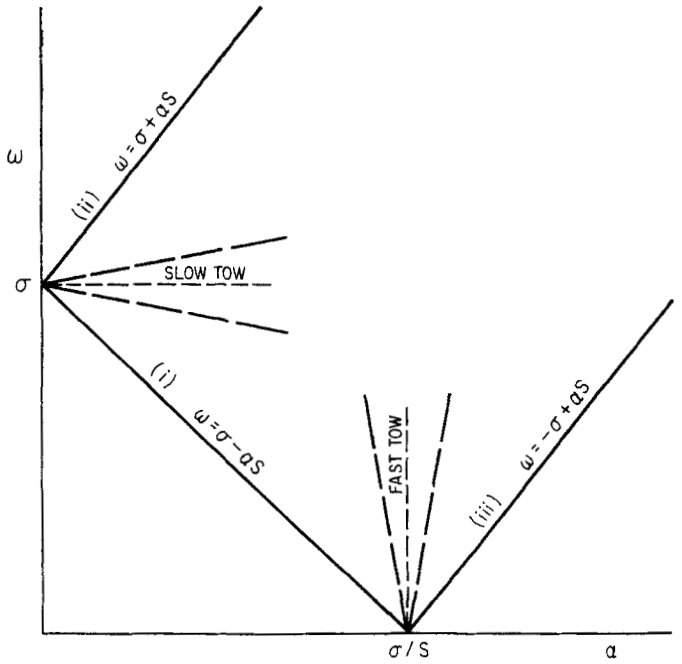

FIGURE 8 Doppler-shifted spectra. Contributions to the spectra at recorded frequency σ for a sensor moving at a constant speed S come from the regions of α, ω-space to the right of the heavy lines, with weighting factor as in Eq. (8.3). For a fast tow, lines (i) and (iii) collapse onto a vertical line $\alpha = \sigma/S$. As the speed approaches zero, (i) and (ii) collapse onto a horizontal line $\omega = \sigma$.

The range $0 \leqq \phi \leqq \frac{1}{2}\pi$ refers to the sector between $\omega = \sigma + \alpha S$ and $\omega = \sigma$; $\frac{1}{2}\pi \leqq \phi \leqq \pi$ covers the area to the right of (i) and (iii). The equivalence of (8.4) and (8.3) can be demonstrated by the substitution of (8.5) and rearrangement of the bounds of integration depending on the order. For a very slow tow the contribution from (iii) vanishes and we may drop the modulus signs

in (8.5) so that (8.4) reduces to (5.5). The velocity spectra behave in just the same way, and so for $S \ll 1$,

$$\hat{F}_u(\sigma) = \pi^{-1}\hat{M}^{-2}\hat{N}\int_0^{\pi} d\phi \int_0^{\infty} \overline{U^2}(\omega, y)E(\alpha, \omega)\, d\alpha, \quad \omega = \sigma + \alpha S \cos\phi. \quad (8.6)$$

SLOW TOW

A pertinent Doppler scale is the phase velocity of the equivalent single mode:

$$S_0 = \frac{\omega}{\frac{1}{2}\mu} \approx \frac{1}{\frac{1}{2}j_i\pi} = 0.032, \qquad \hat{S}_0 = 0.78 \text{ km/h} = 22 \text{ cm/sec}. \quad (8.7)$$

We expect the Doppler effect to be $0(S/S_0)^2$, and this is borne out by the numerical evaluation (Figure 9).

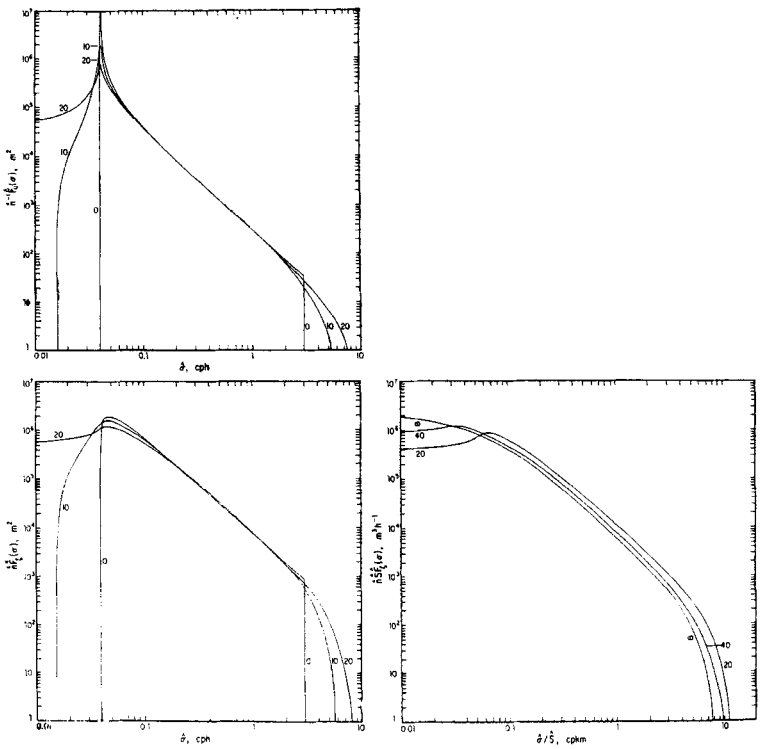

FIGURE 9 Doppler effects on the current spectrum (left) and vertical displacement spectrum (below), for $n = 1$ (3 cph), $E = 2\pi \times 10^{-5}$ (0.38 joules/cm^2), $j_i = 20$. For low speeds the spectra are plotted against frequency-of-encounter $\hat{\sigma}$; for high speeds, against $\hat{\sigma}/\hat{S}$. The curves are for relative speeds $\hat{S}/\hat{S}_0 = 0$, 0.45, 0.90, 1.80, ∞ ($\hat{S} = 0$, 10, 20, 40, ∞ cm/sec) with 0, ∞ corresponding to the moored and towed spectra (6.20, 6.21) respectively.

Typical flow velocity past the mooring† at site D is as follows:

	Shallow	Deep
Computed $\sqrt{\overline{u^2}}$, internal waves, Eq. (6.9)	6 cm/sec	3 cm/sec
Measured monthly mean components, $\frac{1}{2}(\overline{u_1}+\overline{u_2})$	15 cm/sec	3 cm/sec
Measured $\sqrt{\overline{u^2}}$	30 cm/sec	6 cm/sec

Figure 9 shows that speeds greater than 10 cm/sec flatten the inertial cusp of the current spectra and shift appreciable energy to sub-inertial frequencies, in conflict with the observed 20 db drop (Figure 4 and Fofonoff, 1969b). This appears to be a significant constraint on our model, ruling out the possibility of a larger value of j_i.

There is also some shift of energy to frequencies above the buoyancy cut-off. Simple geometric considerations involving Figures 7 and 8 place an upper limit of $\sigma = n(1+2S/S_0)$ to the Doppler-shifted frequencies (taking our model literally) and this would suggest that the observed continuation of the moored spectra well above n is due to other causes (such as fine-structure).

Fast Tow

The main contribution to the towed spectra comes from near ω_μ, involving a velocity $\omega_\mu/\mu = \frac{1}{2}S_0$. We expect the effect of finite "slowness" to be $O(S^{-1}/2S_0^{-1})^2$. It follows that at typical towing speeds the observed wavenumbers do indeed qualify for the "frozen field" approximation (Figure 9). Even at towing speeds as low as 20 cm/sec (0.72 km/h) the effect in the observed wavenumber range (0.1 to 5 cpkm) is merely to raise the spectrum about 2 db.

9. Discussion

Our incentive for this work was to get some hold on the distribution of space *and* time scales of internal waves. Rarely does one see real progress in any field of geophysics if only the space *or* time scales of a phenomenon are appreciated.

† The motion of the mooring is less important in this context. The "compliance" of a submerged float of cross section A with net buoyance B and drag C_D in water at depth h is $k = \frac{1}{2}C_DAh/B$ ($\approx$ 15 sec^2 cm^{-1} for site D, Fofonoff 1966). The horizontal displacement due to a current u = 15 cm/sec is $O(ku^2)$ = 34 m, and in describing 2 circles per day the mooring moves at $\frac{1}{2}$ cm/sec.

Spectra of towed and moored measurements give projections onto the space and time axes, respectively, but these can be satisfied by a broad class of two-dimensional distributions. To narrow the field, we used as our principal tool the observed coherence (or lack thereof) between spatially separated measurements; but then we encountered an incompatibility between the energy spectra and coherence spectra. We could partially suppress this incompatibility by a suitable choice of energy density in the SLOPE region (Figure 7), but this left some further inconsistencies with regard to MH and

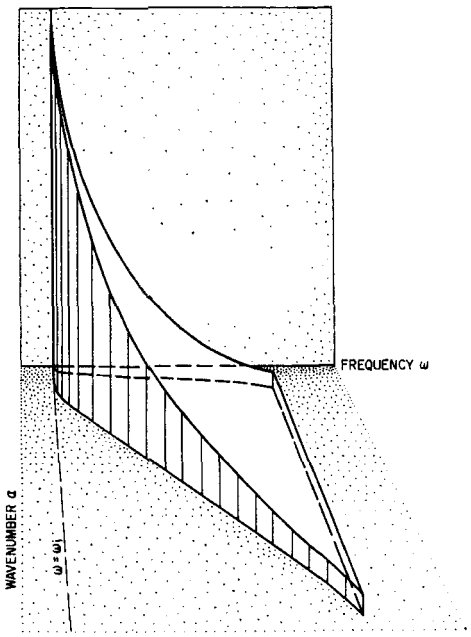

FIGURE 10 A perspective diagram of the energy density $E(\alpha, \omega)$ in wavenumber frequency space. In our model the far side is limited by the dispersion relation of the gravest mode, the near side by a mode of order 20. Both cut-offs are taken as infinitely sharp.

TV coherences. As a way out, we attribute some of the observations to processes other than internal waves, holding the oceanic fine-structure responsible for the loss of coherence between currents separated vertically by tens of meters or less, and for the extension of the moored and towed spectra past the buoyant cut-off.

The space-time model so arrived at is then not inconsistent with the observational evidence as of this moment. The reader will find the model contrived, and we make no claim for uniqueness; but after the many attempts at finding

other models (from which the reader surely wishes to be spared), we have some faith in the essential features (Figure 10): a cusp at the inertial frequency and zero horizontal wavenumber; a monotonic fall-off towards higher frequencies; a wavenumber bandwidth increasing roughly linearly with frequency and equivalent to about 20 modes.

A total energy of roughly 0.4 joules cm^{-2} gives results within an order of magnitude of moored, floating and towed measurements of current and vertical displacement, taken over the years and at many depths off the American west and east coasts, Hawaii, Bermuda and Gibraltar, and in the Bay of Biscay and the Mediterranean. This suggests some universality in the internal wave spectrum, perhaps due to saturation effects like those for surface waves at high frequencies.

Moored and towed spectra may be regarded as asymptotic cases of frequency-of-encounter spectra at zero and infinite towing speeds, respectively; the relevant velocity scale (about 1 km/h for our model) is determined by the wavenumber bandwidth. Our concern is not so much with the finite "slowness" of typical tows, but with the finite drift speed with which internal waves are typically swept by a mooring. In fact, a tow at 1 or 2 knots rapidly sampled would be desirable for extending the towed spectra $F_\zeta(\alpha_1)$ to higher wavenumbers. With regard to $F_\zeta(\omega)$, the technique developed by Voorhis affords the unique opportunity of measuring vertical displacement (not subject to fine-structure noise) from free-floating devices (minimizing Doppler effects).

The urgent need is for measurements from coherent arrays. Table IV relates the vertical and horizontal coherence spacing to the minimum duration of the experiment in order that there be adequate resolution and statistical reliability (we take 20 degrees of freedom as a minimum for geophysical work). The next 10 years will see some efforts, very costly in money and time, towards establishing abyssal arrays. We shall be pleased if our findings can assist in the planning of such experiments.

TABLE IV

Horizontal and vertical coherence scales imposed by bandwidth and fine-structure, at stated frequencies and depth. $T = \frac{1}{2}(20)(\omega-\omega_i)^{-1}$ is the length of record required to resolve a frequency interval $\omega-\omega_i$ with 20 degrees of freedom ($\approx \pm 22\%$)

ω	$\omega_i+0.001$ cph	$\omega_i+0.01$ cph	≈ 0.1 cph	0.3 cph	1 cph	3 cph
X (bandwidth)	20 km	2 km	1800 m	600 m	180 m	60 m
Y (fine-structure)		200 m	100 m	33 m	10 m	3 m
Y (bandwidth) 100 m, 1 km, 5 km } depth	←		{ 40 m, 100 m, 400 m }			→
T	1 year	1 month	100^h	30^h	10^h	3^h

Notation (typical magnitudes)

$\hat{(\ )}$	Dimensional quantities
Superscript $(j) = (1), (2), \ldots$	Mode numbers
Subscripts 1, 2	Horizontal components
Subscripts L, T	Longitudinal and transverse components
Subscripts u, v, ζ	Referring to velocity components and vertical displacement
Subscripts $\hat{d}$ [0.2 km], 0, $\hat{h}$ [4.5 km]	At surface ($y = -d$), "thermocline" ($y = 0$) and bottom ($y = h$)
Subscript i	Pertaining to inertial range
$x(x_1, x_2), y$	Right-handed coordinates, y downwards
$u(u_1, u_2), v; q$	Horizontal and vertical components of velocity; velocity scale
$\zeta(x, y, t)$	Vertical displacement
$U(U_L, U_T), V, Z$	Depth-dependent wave functions
$\alpha(\alpha_1, \alpha_2), \beta$	Horizontal and vertical components of wavenumber
ϕ, θ	Azimuth (relative to x_1) and inclination
$\hat{\omega}, \hat{\sigma}, \hat{\omega}_i$ [0.04 cph]	Frequency, frequency of encounter (at towing speed S), inertial frequency
$n(y)$, $\kappa = \alpha n/\omega$, $a = \alpha(1-\omega_i^2/\omega^2)^{-\frac{1}{2}}$, $k = an/\omega$, $k_0 = a/\omega$, $k_h = an_h/\omega$, $k_i = a^{(1)}(\omega_i)/\omega_i = 2.96$	Väisälä frequency and related notation
$\hat{\rho}(y), \Delta\hat{\rho}$	Basic potential density stratification and scale thereof
$\hat{N} = \hat{n}(0)$ [3 cph], $\hat{n}_h = \hat{n}(h)$ [0.095 cph]	Väisälä frequency at thermocline and bottom
$\hat{b}$ [1.3 km], $\hat{M} = (2\pi\hat{b})^{-1}$ [0.122 cpkm]	Buoyancy scale depth and associated wavenumber
N	Normalization constant
$\hat{E}(\alpha, \omega), \hat{E}(y)$, $\hat{E}$ [0.4 joules cm^{-2}]	Energy per unit wavenumber-frequency and unit area, per unit volume, per unit area
$F(\omega) \propto \omega^{-p}, F(\alpha_1) \propto \alpha_1^{-q}$, $\mu \propto \omega^r$	Moored and towed spectra, α-bandwidth

j_i [20]	j-bandwidth at inertial frequency (Eq. 6.13)
C, Q, R, γ	Co- and quadrature spectra, coherence and phase
X, Y	Horizontal and vertical separations
MC, MV, MH, TV	Moored component, moored vertical, moored horizontal, towed vertical (coherence)
S, S_0 [22 cm/sec = 0.78 km/h]	Towing speed, Doppler scaling
c	A constant

ACKNOWLEDGMENTS

This study has depended largely on measurements by Charnock, Ewart, Fofonoff, Gould, LaFond, Perkins, Pinkel, Voorhis, Webster, and White. Most of the work is recent, and much of it unpublished. We appreciate the opportunity for using the measurements and discussing them with authors, particularly Fofonoff and Webster. Mrs. Greenslate has been most helpful in the preparation of this paper.

REFERENCES

Charnock, H., "A preliminary study of the directional spectrum of short period internal waves," *Proc. 2nd U.S. Navy Symp. Mil. Oceanog.*, 175–178 (1965).

Cox, C., "Internal waves," *The Sea* **1**, 752–763 (1962).

Cox, C., "Energy in semidiurnal internal waves," *Proc. Symp. Mathematical-Hydrodynamical Investigations, Moskau* (1966).

Cox, C., "Internal waves," *Trans. Am. Geophys. Union* **48**, 588–591 (1967).

Cox, C., Nagata, Y. and Osborn, T., "Oceanic fine structure and internal waves," *Bull. Japanese Soc. Fisheries Oceanog.* (UDA Volume), 67–71 (1969).

Cox, C. and Sandstrom, H., "Coupling of internal and surface waves in water of variable depth," *J. Oceanog. Soc. Japan* **20**, 499–513 (1962).

Defant, A., *Physical Oceanography* **2**, Pergamon Press (1961).

Eckart, C., *Hydrodynamics of Oceans and Atmospheres*, Pergamon Press (1960).

Fofonoff, N. P., "Oscillation modes of a deep-sea mooring," *Geo-Marine Technology* **2**, 13–17 (1966).

Fofonoff, N. P., "Spectral characteristics of internal waves in the ocean," *Deep-Sea Research* Suppl. to **16**, 58–71 (1969a).

Fofonoff, N. P., "Role of the NDBS in future natural variability studies of the North Atlantic," *First Science Advisory Meeting*, National Data Buoy Development Project, U. S. Coast Guard (1969b).

Garrett, C. J. R. and Munk, W. H., "Internal wave spectra in the presence of fine-structure," *J. Phys. Oceanog.* **1**, 196–202 (1971).

Gould, W. J., "Spectral characteristics of some current records from the eastern North Atlantic," *Phil. Trans. Roy. Soc.* (in press).

Hendershott, M. C., "A note on Laplace's tidal equations over a yielding earth" (1971) (in preparation).

Kitaigorodsky, S. A., Miropolsky, Yu. Z. and Filyushkin, B. N., "The investigation of statistical structure of the internal wave fields in the ocean" (in preparation).

Krauss, W., "Typical features of internal wave spectra," *Prog. in Oceanog.* **5,** 95–101 (1969).

LaFond, E. C. and LaFond, K. G., "Thermal structure through the California front," Report N.U.C. TP 224, 133 (1971).

Liebermann, L., "The effect of temperature inhomogeneities in the ocean on the propagation of sound," *J. Acoust. Soc. Am.* **23,** 563–70 (1951).

Long, R. R., "A theory of turbulence in stratified fluids," *J. Fluid Mech.* **42,** 349–365 (1970).

Luke, Y., *Integrals of Bessel Functions,* McGraw-Hill (1962).

Martin, S., Simmons, W. F. and Wunsch, C. I., "Resonant internal wave interactions," *Nature* **224,** 1014–1016 (1969).

Monin, A. S. "Specific features of the sea turbulence," *Proc. ICES Symp.* Dublin (1969).

Munk, W. H. and Phillips, N., "Coherence and band-structure of inertial motion in the sea," *Rev. Geophys.* **6,** 447–472 (1968).

Munk, W. H., Snodgrass, F. E. and Wimbush, M., "Tides off shore: transition from California coastal to deep-sea waters," *Geophys. Fluid Dynamics* **1,** 161–235 (1970).

Perkins, H. T., "Inertial oscillations in the Mediterranean" (thesis). M.I.T. and W.H.O.I. (1970).

Phillips, O. M., *The Dynamics of the Upper Ocean,* Cambridge University Press (1966).

Phillips, O. M., "On spectra measured in an undulating layered medium," *J. Phys. Oceanog.* **1,** 1–6 (1971).

Reid, J. L. and Lynn, R. J., "On the influence of the Norwegian-Greenland and Weddell seas upon the bottom waters of the Indian and North Pacific oceans," *Deep-Sea Research* **18,** 1063–1088 (1971).

Schott, F., "On horizontal coherence and internal wave propagation in the North Sea," *Deep-Sea Research* **18,** 291–307 (1971).

Siedler, G., "Vertical coherence of short-periodic current variations," *Deep-Sea Research* **18,** 179–191 (1971).

Stommel, H. and Fedorov, K. N., "Small scale structure in temperature and salinity," *Tellus* **19,** 306 (1967).

Ufford, C. W., "Internal waves measured at three stations," *Trans. Am. Geophys. Union* **28,** 87–95 (1947).

Voorhis, A., "Measurements of vertical motion and the partition of energy in the New England slope water," *Deep-Sea Research,* **15,** 599–608 (1968).

Voorhis, A. D. and Perkins, H. T., "The spatial spectrum of short-wave temperature fluctuations in the near-surface thermocline," *Deep-Sea Research* **13,** 641–654 (1966).

Webster, T. F., "Observation of inertial period motions in the deep sea," *Rev. of Geophys.* **6,** 473–490 (1968a).

Webster, T. F., "Vertical profiles of horizontal ocean currents," *Deep-Sea Research* **16,** 85–98 (1968b).

Webster, T. F., Lectures, *Liege University Second Colloq. on the Hydrodynamics of the Ocean,* 20–53 (1970).

Webster, T. F., "Estimates of the coherence of ocean currents over vertical distances," (1971) (in press).

White, R. A., "The vertical structure of temperature fluctuations within an oceanic thermocline," *Deep-Sea Research* **14,** 613–623 (1967).

Woods, J. D., "Wave-induced shear instability in the summer thermocline," *J. Fluid Mech.* **32,** 791–800 (1968).

Woods, J. D. and Fosberry, G. G., "Observations of the thermocline and transient stratifications made visible by dye," *Proc. 1965 Malta Symp. Underwater Assn.* London (1966).

Zalkan, R. L., "High frequency internal waves in the Pacific Ocean," *Deep-Sea Research* **17,** 91–108 (1970).